Dysregulation of M segment gene expression contributes to influenza A virus host restriction

Brenda M. Calderon[1], Shamika Danzy[1], Gabrielle K. Delima[1], Nathan T. Jacobs[1], Ketaki Ganti[1], Megan R. Hockman[1], Graeme L. Conn[2], Anice C. Lowen[1*], and John Steel[1#*]

Departments of Microbiology and Immunology[1] and Biochemistry[2], Emory University School of Medicine, Atlanta, GA, USA

*Address correspondence to John Steel at john.steel@emory.edu or Anice Lowen at anice.lowen@emory.edu

[#]Current address: Influenza Division, Centers for Disease Control and Prevention, Atlanta, GA, USA

Abstract

The M segment of the 2009 pandemic influenza A virus (IAV) has been implicated in its emergence into human populations. To elucidate the genetic contributions of the M segment to host adaptation, and the underlying mechanisms, we examined a panel of isogenic viruses that carry avian- or human-derived M segments. Avian, but not human, M segments restricted viral growth and transmission in mammalian model systems, and the restricted growth correlated with increased expression of M2 relative to M1. M2 overexpression was associated with intracellular accumulation of autophagosomes, which was alleviated by interference of the viral proton channel activity by amantadine treatment. As M1 and M2 are expressed from the M mRNA through alternative splicing, we separated synonymous and non-synonymous changes that differentiate human and avian M segments and found that dysregulation of gene expression leading to M2 overexpression diminished replication, irrespective of amino acid composition of M1 or M2. Moreover, in spite of efficient replication, virus possessing a human M segment that expressed avian M2 protein at low level did not transmit efficiently. We conclude that (i) determinants of transmission reside in the IAV M2 protein, and that (ii) control of M segment gene expression is a critical aspect of IAV host adaptation needed to prevent M2-mediated dysregulation of vesicular homeostasis.

Author summary

Influenza A virus (IAV) pandemics arise when a virus adapted to a non-human host overcomes species barriers to successfully infect humans and sustain human-to-human transmission. To gauge the adaptive potential and therefore pandemic risk posed by a particular IAV, it is critical to understand the mechanisms underlying viral adaptation to human hosts. Here, we focused on the role of one of IAV's eight gene segments, the M segment, in host adaptation. Comparing the growth of IAVs with avian- and human-derived M segments in avian and mammalian systems revealed that the avian M segment restricts viral growth specifically in mammalian cells. We

show that the mechanism underlying this host range phenotype is a dysregulation of viral gene expression when the avian IAV M segment is transcribed in mammalian cells. In particular, excess production of the M2 protein results in viral interference with cellular functions on which the virus relies. Our results therefore reveal that the use of cellular machinery to control viral gene expression leaves the virus vulnerable to over- or under-production of critical viral gene products in a new host species.

Introduction

Influenza A virus (IAV) epidemics and pandemics result in widespread and often severe disease [1-3], as well as considerable societal economic costs [4]. IAV lineages endemic in humans are ultimately derived from those circulating in wild waterfowl. Sporadic transmission of IAV from avian reservoirs to humans occurs mainly through domesticated intermediate hosts such as chickens and pigs [5]. For example, infection of humans with H7N9 and H5N1 subtype IAVs occurs through direct exposure to infected poultry. Although they often cause severe disease, these zoonotic cases have not led to sustained onward transmission to date and have therefore not caused a pandemic. Despite abundant circulation of IAVs at the animal-human interface, pandemics occur only rarely owing to the host specificity of IAV infection. As with all viruses, IAV must exploit host cell functions and overcome antiviral barriers to execute its life cycle. Viral replication in a new host species therefore requires adaptation to re-establish virus-host interactions broken by species-specific features of host cellular processes. IAV can undergo such adaptation through reassortment of intact gene segments between avian IAVs and those already adapted to mammals or through more incremental changes brought about by polymerase error [6]. With the goal of anticipating and mitigating IAV emergence in humans, it is essential to understand the species-specific barriers to infection and the mechanisms by which IAV evolution allows these impediments to be overcome.

67 Changes to viral receptor specificity and polymerase function necessary to overcome host
68 species barriers have been well documented [7-11], but it is clear that additional features of
69 avian IAVs restrict their growth in mammalian systems [12-14]. Seminal studies, performed in
70 the 1970s, indicated a potential role for the M segment. Avian IAVs were shown to express low
71 levels of M1 protein during abortive infection of mammalian cells, but not avian cells [15-17],
72 and the limited quantity of viral particles formed during such abortive infections correlated with
73 the amount of M1 protein expressed. Significantly, these studies were conducted prior to the
74 identification of a second gene product expressed from a spliced form of the M segment mRNA:
75 the M2 protein [18,19]. Subsequent studies demonstrated that low M1 expression during
76 abortive avian IAV infection in mammalian cells was accompanied by increased M2 mRNA and
77 protein expression, relative to productive infection in avian cells, leading to new hypotheses
78 regarding the mechanisms leading to abortive outcomes [20-22].
79 Additional evidence for a role of the M segment in host range comes from the *in silico*
80 identification of positive selection acting on the M segment of the Eurasian avian-like swine
81 lineage, following transfer of this IAV from birds to swine [23]. Moreover, others and we have
82 shown that the M segment of the 2009 pandemic H1N1 (pH1N1) strain carries determinants of
83 transmissibility, suggesting that adaptation of this segment to humans contributed to the
84 emergence of the pH1N1 lineage [24-28]. The mechanistic basis for this contribution; the
85 specific roles, if any, of M1 and M2 proteins to host range; and whether the M segment plays a
86 broader role in IAV host adaptation, remain unclear.
87 It is now recognized that the M segment of IAV encodes the M1 matrix and the M2 proton
88 channel proteins via alternative splicing (**Suppl. Figure 1A)** [29,30]. M1 forms a structural layer
89 under the viral envelope and is a major determinant of virion morphology [24,26,31,32]. Upon
90 endocytosis of virus particles into cells, low pH and high [K+] trigger a conformational change in
91 M1 required for release of viral ribonucleoprotein (vRNP) complexes into the cytoplasm [33]. M1
92 is also critical for the transport of newly replicated vRNPs from the nucleus to the cytoplasm [34-

93 37]. At late stages of infection, cytoplasmic M1 is thought to recruit vRNP complexes to the
94 budding site [38-40].
95 M2 is a transmembrane protein that tetramerizes to form a proton channel. Within the envelope
96 of incoming virions, this channel allows diffusion of protons into the virion core, thereby
97 triggering the release of vRNPs from M1, as well as facilitating the intracellular transport of HA
98 protein [41-44]. M2 also plays an important role in the final stages of virion morphogenesis,
99 mediating ESCRT-independent membrane scission [45]. Importantly for the findings reported
100 herein, multiple groups have reported that M2 blocks the fusion of autophagosomes with
101 lysosomes [46-48]. Under normal conditions, this fusion event allows degradation and recycling
102 of organelles and protein aggregates contained within autophagosomes [49], and is thus
103 important for cellular homeostasis. M2-mediated interference with autolysosome formation
104 therefore stalls autophagic flux and leads to the accumulation of autophagosomes within the cell
105 [46-48].
106 Many elegant molecular virology studies have revealed that viral strategies for regulating gene
107 expression are central to orchestration of the viral life cycle [50-53]. Here, we report that
108 regulation of M2 expression of IAV is an important determinant of host range. In particular, our
109 data show that the expression of M1 and M2 from alternatively spliced M segment mRNAs is
110 dysregulated when an avian IAV replicates in mammalian cells, and that the resultant
111 overexpression of the M2 proton channel attenuates viral growth by disrupting the cellular
112 autophagy pathway. The observed block in autophagy is consistent with that reported previously
113 for lab-adapted strains of IAV [46-48]. Importantly, however, we see that lab-adapted IAVs
114 express M2 at high levels, comparable to those seen for avian IAV M segments in mammalian
115 cells. In contrast, IAVs carrying M segments well adapted to mammalian systems express
116 relatively little M2 and do not trigger the accumulation of autophagosomes to the same extent as
117 avian-origin and lab-adapted strains. These findings suggest that IAV-induced stalling of
118 autophagic turnover is a result of aberrantly high M2 expression upon infection of mammalian

119 cells with avian IAVs, and which is overcome in human-adapted influenza A lineages. Critically,
120 the mechanism leading to this host-restricted phenotype occurs at the level of gene expression
121 and is driven by host-specific differences in viral nucleic acid sequence, not amino acid changes.
122 This mechanism constitutes a novel paradigm in RNA virus host adaptation, and reveals a new
123 species barrier for IAV, which may be highly relevant for the emergence of avian IAVs into
124 humans.
125
126 **Results**
127 **Generation of isogenic IAVs differing only in the M segment**
128 To assess the contribution of the M segment to host adaptation, we generated a panel of IAVs
129 possessing human- or avian-derived M segments in the A/Puerto Rico/8/34 (H1N1) [PR8]
130 background (**Table 1; Figure 1A; Suppl. Figure 1B, C, D**). The M segments used were
131 selected with the aims of representing circulating human IAVs and capturing the breadth of
132 diversity of M segment sequences present in wild waterfowl. In addition to three wild-type avian
133 M segments, we included in our panel a mutant of the dk/Alb/76 M segment that carries a
134 uniquely identified mutation in M2 (S89). Reversion of this unique amino acid residue to glycine
135 yields an M2 protein matching the consensus amino acid sequence of IAVs in wild bird
136 reservoirs. The human-adapted M segment analyzed most extensively herein is that of the
137 pandemic A/NL/602/09 (H1N1) strain [NL09].
138
139 **Table 1. Origin of IAV M segments used in study**

Strain	Abbreviation	% Nucleotide identity to avian H1N1 subtype consensus	% M1 a.a. identity to avian consensus (no. of differences)	% M2 a.a. acid identity to avian consensus (no. of differences)
A/NL/602/2009 (H1N1)	NL09	91.7	96.4 (9)	92.8 (7)
A/Panama/2007/99 (H3N2)	Pan99	91.0	95.6 (11)	85.6 (14)
A/Bethesda/55/2015 (H3N2)	Beth15	90.5	95.6 (11)	83.5 (16)
A/mallard/MN/19906/99 (H3N8)	MallMN99	98.9	100	97.9 (2)

A/rhea/North Carolina/39482/93 (H7N1)	RhNC93	98.7	100	100
A/duck/Alberta/35/76 (H1N1)	DkAlb76	96.6	100	99 (1)
A/duck/Alberta/35/76 (H1N1) M2 89G	DkAlb76 89G	96.7	100	100

a.a.: Amino acid residue.

IAV M segments of avian origin confer a host-restricted phenotype

The relative fitness of PR8-based viruses carrying M segments from the human-adapted NL09 virus or from avian IAVs was evaluated in three avian substrates: embryonated chicken eggs (ECE), chicken origin DF-1 cells, and quail origin QT-6 cells. When grown from low multiplicities of infection (MOI) in either ECE or DF-1 cell substrates, all viruses exhibited similar kinetics and reached comparable titers (**Figure 1B and 1C**). Also, under high MOI growth conditions in DF-1 and QT-6 cells, the growth phenotypes of the PR8 NL09 M and PR8 avian M viruses were similar, although the NL09 M-containing virus trended towards increased growth relative to the avian M-containing viruses in DF-1 cells (**Figure 1D and 1E)**. Nonetheless, at no time did the NL09 M-encoding virus grow to significantly higher titers than the avian M-encoding viruses in any avian host substrate. In contrast, in mammalian cells, human-adapted IAV M segments were found to support improved growth relative to avian-adapted M segments. Viral growth was monitored from low and high MOI in human A549 cells and canine MDCK cells (**Figure 2**), and additionally from high MOI in human 293T cells (**Suppl. Figure 2A**). In each case, PR8-based viruses carrying the NL09 M segment grew with more rapid kinetics and to higher titers than isogenic viruses carrying avian M segments, although the differences in growth from low MOI did not reach statistical significance. To extend our findings to an independent human lineage of IAV, we evaluated the growth from high MOI in A549 cells of PR8 Pan99 M and PR8 Beth15 M viruses, each of which have an M segment derived from the human seasonal H3N2 lineage (**Suppl. Figure 1C, D**). We found that both of these human-adapted M segments supported significantly faster kinetics and higher magnitude of growth than the dkAlb76 89G M segment (**Suppl. Figure 2B**). Thus, results from multiple different avian and mammalian culture systems reveal defects in the kinetics and magnitude of viral growth associated with avian IAV M

164 segments specifically in mammalian host cells and provide evidence of the acquisition of
165 adaptive changes in the M segment of pH1N1 and H3N2 human influenza A lineages.
166
167 **Avian IAV M segments confer lower viral infectivity, growth and transmission than NL09**
168 **M segment in a guinea pig model**
169 To evaluate the impact of M segment host adaptation on viral phenotypes in an intact host, we
170 evaluated the PR8 NL09 M virus and the four PR8-based viruses carrying avian M segments in
171 a guinea pig model [54,55]. A low inoculation dose of 10 PFU per animal was used to maximize
172 the sensitivity of the system. Each inoculated animal was co-caged with a naïve guinea pig at
173 24 h post-inoculation and viral infectivity, magnitude and kinetics of growth, and transmission
174 were monitored by collecting nasal lavage samples every other day. Among those animals that
175 were productively infected, total virus sampled in nasal washes over the course of infection was
176 evaluated by calculating the area under the shedding curves shown in **Figure 3A**. Area under
177 the curve values did not differ significantly among the four viruses with avian M segments, but
178 were significantly higher for PR8 NL09 M virus (**Figure 3A**). As shown in **Figure 3B**, fewer
179 guinea pigs were productively infected with 10 PFU when the inoculating virus carried an avian
180 M segment. Differences in the kinetics of viral growth were determined by assessing changes in
181 growth over time using repeated measures ANOVA (**Suppl. Figure 3**). Each virus encoding an
182 avian host-derived M segment replicated with significantly slower kinetics than the PR8 NL09 M
183 virus.
184 The efficiency of transmission was assessed by calculating the proportion of contact animals
185 that contracted infection, considering only cages in which donor guinea pigs were productively
186 infected through intranasal inoculation. While transmission occurred in 7/9 instances for PR8
187 NL09 M virus, a significantly lower proportion of animals (1/20; $p<0.0001$) were infected with a
188 virus carrying an avian M segment transmitted from her cage mate (**Figure 3B**). Thus, data from
189 a mammalian animal model reveal defects in infectivity, growth and transmission associated

190 with avian IAV M segments. Our results suggest the acquisition of adaptive changes in the M
191 segment of pH1N1 human IAV since its introduction from the avian reservoir into mammals.
192
193 **The M2 proton channel is aberrantly overexpressed from avian IAV M segments in**
194 **mammalian cells**
195 To investigate the mechanism underlying the host-restricted phenotypes conferred by avian-
196 adapted M segments, the steady state levels of the M1 and M2 proteins were evaluated in
197 human A549 and avian DF-1 cells infected at high MOI. Western immunoblotting with the
198 monoclonal antibody E10, which recognizes the shared N-terminus of M1 and M2, was used to
199 monitor levels of both proteins concurrently.
200 In the avian cell line, the PR8 NL09 M virus expressed lower levels of M2 than M1 (**Figure 4A**).
201 When M1 and M2 levels were normalized to those of vinculin and the relative levels of M1 and
202 M2 calculated, the NL09 M2 protein comprised <10% of the total M segment-derived protein
203 expression. Very similar results were seen for four PR8-based viruses carrying avian M
204 segments grown in DF-1 cells. In each case, M2 comprised <20% of the total M segment-
205 derived protein, and in the case of three avian M segment-containing viruses (PR8 dkAlb76 M;
206 PR8 dkAlb76 M 89G; and PR8 rheaNC93 M), the levels of M1 and M2 proteins were not
207 significantly different from those expressed by the PR8 NL09 M virus (**Figure 4B, 4C, 4D**).
208 In A549 cells, the PR8 NL09 M virus expressed M2 at ~20% of the total M protein, similar to the
209 expression levels observed in infected DF-1 cells (**Figure 5A**). In contrast, avian M segments
210 yielded markedly higher levels of the M2 protein than were observed for the same viruses grown
211 in avian cells. Here, M2 levels were approximately equal to those of M1 (**Figure 5B, 5C, 5D**).
212 Moreover, when compared to the NL09 M segment in human cells, levels of M2 protein were
213 significantly higher for avian M segments ($P<0.0001$) (**Figure 5C, 5D**). Thus, compared to
214 matched virus-host pairings in both human and avian systems, M2 was markedly
215 overexpressed when avian-adapted M segments were introduced into human cells.

216

217 **Overexpression of M2 protein in mammalian cells corresponds to increased levels of the**
218 **M2 mRNA (mRNA 10)**

219 The M segment vRNA is transcribed by the viral polymerase to give rise to a co-linear mRNA
220 ($mRNA_7$), which can be spliced by cellular splicing factors to yield $mRNA_{10}$ or $mRNA_{11}$ [18,56].
221 The M1 protein is translated from the unspliced $mRNA_7$, while M2 is expressed from the spliced
222 $mRNA_{10}$. To date, no polypeptide corresponding to the short $mRNA_{11}$ ORF has been identified.
223 Aberrantly high levels of IAV $mRNA_{10}$ in mammalian cells have been previously reported for the
224 avian IAV, fowl plague virus [20,21]. We therefore hypothesized that the high expression levels
225 of M2 protein, observed for avian-adapted M segments in human cells, was due to increased
226 splicing of $mRNA_7$ to yield excessive $mRNA_{10}$. We used a RT primer extension assay to quantify
227 the levels of each M segment-derived mRNA species in DF-1 and A549 cells infected with either
228 PR8 NL09 M virus or one of four viruses carrying an avian-adapted M segment.

229 As expected, based on the levels of the encoded proteins, $mRNA_{10}$ was of low abundance
230 compared to $mRNA_7$ for all viruses in DF-1 cells (**Figure 6A**). Quantification of band intensities
231 revealed that, in DF-1 cells infected with PR8 NL09 M virus, $mRNA_7$ comprised ~75%, while
232 $mRNA_{10}$ comprised ~5% of the total M segment-derived mRNA (**Figure 6B**). For three avian M
233 viruses (PR8 dkAlb76 M; PR8 dkAlb76 M 89G; and PR8 rheaNC93 M), relative levels of $mRNA_7$
234 were ~70-75% and were not significantly different from those of PR8 NL09 M virus (**Figure 6B**).
235 For all viruses, $mRNA_{10}$ was expressed at low levels (10-40% of total segment 7 mRNA), and in
236 the case of two avian M segment-containing viruses (PR8 dkAlb76 M; PR8 dkAlb76 M 89G), the
237 levels of $mRNA_{10}$ were not significantly different from those expressed by the PR8 NL09 M virus
238 (**Figure 6C**). $mRNA_{11}$ was expressed in each infection at approximately 20% of the total M
239 segment-derived mRNA, and the relative level did not differ significantly with any virus (**Figure**
240 **6D**). Overall, the relative levels of each of the three mRNA species were similar when

241 synthesized from avian- or human-origin encoded M segments in DF-1 cells, correlating with
242 Western immunoblot data on M segment protein expression in these cells.
243 In A549 cells, the PR8 NL09 M virus showed relatively high abundance of $mRNA_7$ and low
244 abundance of $mRNA_{10}$, as was seen in DF-1 cells (**Figure 7A**). By contrast, for viruses carrying
245 avian-adapted M segments, $mRNA_{10}$ levels exceeded those of $mRNA_7$ in A549 cells (**Figure 7B,**
246 **7C**). Both decreases in $mRNA_{10}$ levels and increases in $mRNA_7$ levels contributed to the altered
247 relative abundance. Again, no significant differences in relative $mRNA_{11}$ levels among the
248 viruses were noted (**Figure 7D**) suggesting that changes in splicing to produce $mRNA_{11}$ do not
249 contribute to changes in M segment mRNA and protein expression observed in A549 cells.
250 Overall, our data point to increased splicing to produce $mRNA_{10}$ as the underlying mechanism
251 leading to heightened M2 expression from avian M segments in A549 cells, and suggest that
252 cis-acting signals present on the M segment are responsible for driving the disparate M2
253 expression levels.
254
255 **M2 expressed from avian M segments localizes in perinuclear puncta**
256 To gain initial insight into the phenotypic consequences of M2 overexpression, we examined the
257 subcellular localization of M2 in A549 cells infected with PR8 NL09 M virus or one of four PR8-
258 based viruses with avian M segments. At 8 hours-post-infection (hpi) in PR8 NL09 M virus-
259 infected cells, M2 showed mainly dispersed cytoplasmic staining, along with weak cytoplasmic
260 membrane localization and some perinuclear accumulation. By contrast, in cells infected with
261 viruses that encoded any of the four avian origin M segments, we noted more abundant M2
262 protein staining localized at the plasma membrane, and in large puncta near the cell nucleus
263 (**Figure 8A**). Similar data were obtained from virus-infected 293T cells at 8 hpi (**Figure 8B**) and
264 from both human cell lines at 12 hpi (**Suppl. Figure 6**). This staining pattern, along with data in
265 previously published studies [46-48], prompted us to investigate whether highly expressed M2
266 protein was interacting with the cellular autophagy pathway.

267

268 **Human cells exhibit increased LC3B II levels when infected with IAV carrying avian M**
269 **segments**

270 An interaction between the IAV M2 protein and the cellular autophagy pathway has been
271 reported previously [46-48]. To test whether M2 expression from avian vs. human M segments
272 has differential effects on autophagy, we first evaluated the level of LC3B lipidation in PR8 NL09
273 M- and PR8 avian M-infected cells. Upon activation of the autophagy pathway, LC3B is modified
274 through the addition of phosphotidylethanolamine [57,58]. This lipidated form, called LC3B II,
275 remains associated with the membranes of maturing and mature autophagosomes. Thus,
276 increased levels of LC3B II in the cell are indicative of autophagosome formation; however,
277 under normal conditions LC3B I and II are cycled through an autophagic flux which involves
278 autophagosome maturation and degradation via fusion with lysosomes [59]. A block in this
279 fusion event can therefore lead to accumulation of autophagosomes in the cytoplasm and,
280 consequently, accumulation of LC3B II in the cell.

281 Western immunoblot analysis of LC3B revealed decreased LC3B I and increased LC3B II
282 protein levels in virus-infected cells compared to mock, providing evidence of autophagy
283 activation and/or block during IAV infection of either avian or human cells (**Figure 4A, 4E, 4F;**
284 **5A, 5E, 5F**). In avian DF-1 cells, levels of LC3B I were slightly decreased and levels of LC3B II
285 were slightly increased over mock, but LC3B I and LC3B II levels were generally comparable
286 among human M- and avian M-containing viruses (**Figure 4E, 4F**). Importantly, human A549
287 cells infected with PR8 avian M-containing viruses consistently showed lower levels of LC3B I,
288 and higher levels of LC3B II than A549 cells infected with PR8 NL09 M as well as other human
289 M-containing viruses (**Figure 5E, 5F).** Additionally, the same phenotypes were obtained from
290 the panel of viruses upon infection of human origin 293T cells (**Suppl. Figure 4A-4F**), or canine
291 origin MDCK cells (**Suppl. Figure 4G-4L**).

292 Taken together, these data reveal a correlation between levels of M2 expression and LC3B
293 lipidation (accumulation of LC3B II), suggesting that high levels of M2 present in PR8 avian M-
294 infected cells may be inducing an over-activation of autophagy, or a block in the turnover of
295 autophagosomes.
296
297 **Infection of human cells with IAV carrying avian M segments triggers accumulation of**
298 **autophagosomes**
299 To confirm that M2 protein was co-localizing with LC3-positive autophagic vesicles in
300 mammalian cells, we monitored sub-cellular localization of an overexpressed LC3B-GFP fusion
301 protein in infected cells. Human 293T cells were primarily used for this purpose as they
302 transduce well with GFP-LC3. Under normal conditions, LC3B-GFP can be seen throughout the
303 cell with a diffuse distribution (**Figure 9, row 1: mock infected cells**). Treatment with
304 chloroquine, an inhibitor of autophagy that decreases autophagosome-lysosome fusion, results
305 in the concentration of LC3B-GFP into punctate cytoplasmic structures (**Figure 9, row 7: CQ-**
306 **treated cells**). This relocalization is indicative of the accumulation of autophagosomes [60]. In
307 LC3B-GFP expressing 293T cells infected with PR8 NL09 M virus, we observed little to no
308 increase in GFP-positive cytoplasmic puncta (**Figure 9, row 2: NL09 M infected cells**). In cells
309 infected with PR8 avian M-encoding viruses, by contrast, extensive accumulation was apparent,
310 with both the size and number of intracellular vesicles increased relative to PR8 NL09 M
311 infection (**Figure 9, rows 3-6: Avian M infected cells**). In addition to these cytoplasmic puncta,
312 viruses with avian M segments were found to redirect a small proportion of LC3B-GFP to the
313 plasma membrane. Notably, the M2 protein co-localized with LC3B-GFP in PR8 avian M-
314 infected cells, both in cytoplasmic puncta and at the plasma membrane. Similar phenotypes
315 were observed in virus-infected A549 cells, at 8 hpi **(Suppl. Figure 7**). Overall, these results
316 suggest that expression of avian M2 protein at high levels interferes with the turnover of

317 autophagosomes and with the localization of LC3B-GFP. In addition, the results reveal a
318 reduction in the tight perinuclear localization of M2 upon LC3B overexpression.
319 As an additional test designed to differentiate autophagy induction from autophagy block in cells
320 infected with IAV carrying avian M segments, we used chloroquine treatment followed by
321 Western immunoblotting for LC3B I and LC3B II. We hypothesized that, if autophagic flux is
322 blocked in cells infected with PR8 avian M viruses, then treatment with chloroquine would not
323 lead to a further increase in LC3B II levels. Conversely, if virus infection of these cells induces
324 autophagy, then blocking their turnover with chloroquine would result in heightened LC3B II over
325 mock-infected, chloroquine-treated cells. As shown in **Suppl. Figure 8A and 8C**, we observed a
326 significant difference in the activation of LC3B II following infection with human- or avian M-
327 encoding viruses. This difference in LC3B II activation is lost in the presence of chloroquine.
328 Additionally, as we observed no change in LC3B II levels upon treatment of virus-infected cells
329 with chloroquine, relative to chloroquine-treated, mock-infected cells, we conclude that the high
330 levels of IAV M2 protein expressed from avian M segments, but not human M segments,
331 precipitate a block in the autophagy pathway such that chloroquine treatment cannot bring
332 about further accumulation of autophagosomes.
333
334 **Ion channel activity of IAV M2 contributes to LC3B II accumulation in A549 cells**
335 To evaluate the contribution of IAV M2 ion channel activity to the observed stalling of autophagy
336 in PR8 avian M virus-infected cells, we inhibited channel activity with amantadine [61].
337 Amantadine was added at 1 hpi and the level of LC3B lipidation was assessed at 8 hpi in PR8
338 NL09 M and PR8 avian M virus-infected A549 cells. The timing of amantadine addition was
339 designed to avoid disruption of the early function of M2 in delivery of the viral genome to the
340 cytoplasm, but allow inhibition of M2 activity in autophagosomes.
341 As noted above (**Figure 5; Suppl. Figure 4**), Western immunoblot analysis of LC3B revealed
342 decreased LC3B I and increased LC3B II upon infection of A549, 293T or MDCK cells, with

343 avian or human M-encoding IAV, with the effect being stronger for viruses possessing avian M
344 segments. Interestingly, addition of amantadine reversed the intracellular accumulation of LC3B
345 II in both human and avian M-infected A549 cells (**Figure 10**). Quantitation of M segment-
346 encoded proteins by Western immunoblot analysis showed no difference in the expression
347 levels of M1 or M2 protein upon treatment with amantadine (**Figure 10 A, 10B, 10C, 10D**), but
348 revealed a statistically significant increase in LC3B I (**Figure 10E**) and decrease in LC3B II
349 (**Figure 10F**) to levels comparable to mock-infected cells.
350 To ensure that the amantadine was working to prevent LC3B II accumulation through inhibition
351 of M2 ion channel activity, we assessed the impact of amantadine treatment on the inhibition of
352 phagosome-lysosome fusion by chloroquine. Amantadine had no impact on LC3B II
353 accumulation in the absence of M2 protein (**Figure 10G-I**), indicating that the mechanism of
354 amantadine block of autophagosome accumulation was specifically mediated through
355 interference with M2 function.
356 As a complementary approach to monitor the effects of amantadine, we again used
357 overexpressed LC3B-GFP fusion protein in infected 293T cells at 12 hpi. Using confocal
358 microscopy, we tracked LC3B-GFP localization in the presence and absence of the ion channel
359 blocker. In line with the Western immunoblot analyses obtained in A549 cells, we saw that
360 amantadine reduced the accumulation of LC3B-GFP within cytoplasmic puncta and at the
361 plasma membrane of infected cells (**Figure 11**). Of note, amantadine treatment did not alter
362 levels or localization of M2 protein and, moreover, had no detectable effect on LC3B-GFP
363 appearance in chloroquine-treated cells (**Figure 11**).
364 Overall, our results indicate that the intracellular ion channel activity of IAV M2 protein is
365 necessary to mediate the observed block in autophagy, and that addition of amantadine can
366 reverse the autophagic phenotypes induced by both human and avian M-encoding IAVs.
367

368 **Improved viral growth in the presence of amantadine implicates autophagy block in viral**
369 **growth restriction**

370 To test for a causal link between the observed block in autophagy and the restriction of growth
371 seen for PR8 avian M-encoding viruses in mammalian cells, we monitored the effect on viral
372 growth of relieving the autophagy block with amantadine treatment. Specifically, we evaluated
373 single-cycle growth in A549 cells using PR8 NL09 M and PR8 dkAlb76 M 89G viruses.
374 Amantadine was again added at 1 hpi to avoid disruption of the earliest steps of the viral life
375 cycle. While amantadine had no effect on growth of the PR8 NL09 M virus (P=0.271), a modest
376 but consistent increase in the titer of PR8 dkAlb76 M 89G virus was noted throughout the time-
377 course (P=0.0007) (**Figure 12**). This result indicates that M2 ion channel-induced disruption of
378 vesicular homeostasis contributes to the host restriction conferred by avian IAV M segments.

379

380 **Viral growth restriction and autophagy block are linked to M2 expression levels, not**
381 **amino acid sequence**

382 To determine whether the observed effects of avian-origin M segments on the viral life cycle and
383 the autophagy pathway are attributable to avian-adapted amino acid sequences or rather to the
384 overexpression of the viral proton channel, we generated a series of chimeric M segments in
385 which the coding changes found in the NL09 M segment were transferred to an avian-adapted
386 RNA background, and vice versa. We introduced all 16 coding changes into M1 and M2
387 simultaneously, or introduced only the nine or seven changes into M1 or M2, respectively. The
388 genotypes of this panel of six chimeric viruses are outlined in **Table 2** and **Suppl. Figure 9**.

389

390 **Table 2. Genotypes of avian-human chimeric M segments**

	Nucleic acid background	M1 amino acid sequence	M2 amino acid sequence
NL M 16mut	NL09 M	Avian consensus M1	Avian consensus M2
NL M 9mut	NL09 M	Avian consensus M1	NL09 M2
NL M 7mut	NL09 M	NL09 M1	Avian consensus M2
Av M 16mut	Dk Alb 76 M 89G	NL09 M1	NL09 M2

Av M 9mut	Dk Alb 76 M 89G	NL09 M1	Avian consensus M2
Av M 7mut	Dk Alb 76 M 89G	Avian consensus M1	NL09 M2

Western immunoblot analysis of M1 and M2 proteins expressed from these six chimeric M segments in infected A549 cells is shown in **Figure 13A**. Among the viruses with the NL09 M nucleic acid background, the PR8 NL M 16mut and PR8 NL M 9mut viruses both showed increased levels of M2 relative to the PR8 NL09 M virus control, indicating that all or some of the coding changes introduced into the M1 ORF impact regulation of M2 gene expression. The PR8 NL M 7mut virus showed similar M1 and M2 expression levels as the PR8 NL09 M control, however. This virus therefore expresses the avian consensus M2 protein at low levels. All viruses with the nucleic acid background of the avian M segment showed relatively high levels of M2, similar to those seen for the PR8 dkAlb76 M 89G virus control. Thus, in the avian nucleic acid background, we were able to fully separate M2 expression level from M2 and M1 amino acid sequence.

Single-cycle growth analysis of the chimeric viruses in A549 cells revealed a strong correlation between M2 expression level and viral yields (**Figure 14A, B and C**). Notably, all viruses with the dkAlb76 M 89G-derived nucleic acid background, which express high levels of M2 protein, grew to approximately 10-fold lower titers than the PR8 NL09 M virus, despite expression of NL09 M1 and/or M2 proteins. In addition, the PR8 NL M 7mut virus, which expresses the human M1 and avian M2 proteins at levels typical of human-adapted strains, showed equivalent growth to that seen with the PR8 NL09 M virus, indicating that amino acid changes in M2 are not required for efficient replication in human cells. Notably, the PR8 Av M 9mut virus, which encodes identical M1 and M2 proteins as PR8 NL M 7mut virus (**Suppl. Figure 9**), exhibits approximately 10-fold reduced viral replication relative to PR8 NL M 7mut virus (P=0.0003) (**Figure 14B and C**). This result confirms that overexpression of M2 protein is a dominant negative trait that is deleterious to virus growth.

415 Examination of LC3B lipidation by Western immunoblot analysis also revealed a clear
416 correlation between M2 expression levels and those of LC3B II within infected cells (**Figure**
417 **13A**). Importantly, overexpression of either human or avian M2 during infection boosted LC3B II
418 levels (compare lanes 2, 3, 5, 6, 7 and 8 in **Figure 13A**), while expression of avian M2 at levels
419 comparable to those of PR8 NL09 M virus gave low LC3B II levels (compare lanes 1 and 4 in
420 **Figure 13A**). Confocal images of 293T cells transduced with LC3B-GFP and infected with the
421 chimeric viruses were consistent with these findings. As seen for wild-type avian M segments,
422 high M2 expression again led to the accumulation of LC3B-GFP in perinuclear puncta and at the
423 plasma membrane (**Suppl. Figure 10**). Thus, as with viral growth, the accumulation of
424 autophagosomes within infected cells appears to be triggered by high levels of M2, regardless
425 of amino acid sequence.
426 To verify that the levels of M1 and M2 protein exhibited by the chimeric M segment-encoding
427 viruses are modulated at the level of mRNA expression, we conducted RT primer extension
428 assays. These data confirmed that differences in the levels of segment 7 mRNA expression
429 (**Suppl. Figure 11**) mirrored the observed differences in M1 and M2 protein expression levels.
430 Overall, these data support the premise that splicing signals are at least partly encoded in non-
431 synonymous nucleotide changes residing in the M1 ORF.
432
433 **Chimeric M segment expressing NL09-like levels of NL09 M1 and avian M2 supports**
434 **robust growth *in vivo***
435 To evaluate whether correcting expression of the avian M2 protein to levels seen for viruses
436 with human-adapted M segments yielded a well-adapted phenotype in a mammalian animal
437 model, we evaluated growth and transmission of PR8 NL09 M 7mut virus in guinea pigs.
438 Titration of nasal wash samples revealed that the PR8 NL09 M 7mut virus (which expresses
439 avian M2 at low levels) had a similar growth phenotype to that of PR8 NL09 M virus: growth
440 kinetics and area under the curve values were not significantly different (**Figure 15; Suppl.**

441 **Figure 12**). In contrast, analysis of nasal wash samples collected from contact animals
442 indicated that only one of eight inoculated guinea pigs transmitted the PR8 NL09 M 7mut virus
443 to her cage mate. This level of transmission is significantly decreased relative to the PR8 NL09
444 M virus (P=0.0339) (**Figure 3B**). Taken together, these results indicate that, when expressed at
445 levels typical for a human-adapted M2 protein, an avian M2 supports efficient replication but
446 inhibits transmission in a mammalian host.
447

448 **Lab-adapted IAV, but not recent human isolates, express abundant M2 and block**
449 **autophagy in human cells**

450 The M2-induced block in autophagic flux reported previously was based on multiple IAVs that
451 were originally isolated from human hosts but passaged extensively in laboratory substrates
452 [46-48]. To assess whether these prior data were consistent with our own, we compared M2
453 expression levels exhibited by one of the lab-adapted strains used, PR8. Our results show that
454 the relative expression levels of M1 and M2 in PR8-infected 293T cells are comparable to those
455 seen in cells infected with avian M-encoding viruses (**Suppl. Figure 13**). These results suggest
456 that prior reports of M2-induced block in autophagy reflect a feature of mal-adaptation to the
457 host cell.
458

459 **Discussion**

460 Our data indicate that dysregulation of gene expression from the IAV M segment contributes to
461 the limited replicative capacity of avian IAVs in mammalian hosts. When transcribed within
462 mammalian cells, avian IAV M segments gave rise to abundant $mRNA_{10}$ and correspondingly
463 high levels of the encoded M2 proton channel. Comparison to matched virus-host systems
464 indicated that this M2 expression profile was an aberrant feature of avian IAV replication in
465 mammalian cells. When present at high levels, M2 had marked effects on the infected cell,
466 blocking the turnover of autophagic vesicles and redirecting LC3B II, the activated form of a

467 critical autophagy mediator, to the plasma membrane. These effects were found to rely on the
468 proton channel activity of M2 and occurred when either the avian or human M2 protein was
469 overexpressed in infected cells. Importantly, the reduction in viral growth conferred by avian M
470 segments in mammalian systems could be attributed at least in part to disruption of vesicular
471 homeostasis and was fully attributed to the altered expression levels of M1 and M2. Thus, our
472 data identify the regulation of viral gene expression as a novel host-dependent feature of the
473 IAV lifecycle that contributes to the host range restriction of this virus (**Figure 16**).
474 Quantification of IAV encoded mRNAs within infected cells indicated that overexpression of M2
475 from avian IAV M segments stems from over-production of the corresponding mRNA. M2 is
476 encoded by the $mRNA_{10}$ transcript, which is generated through splicing of the M1 message,
477 $mRNA_7$ [18,56]. Thus, regulation of M2 gene expression is intimately linked to the cellular
478 splicing machinery. Our data indicate that this is a finely balanced interaction between IAV and
479 its host cell, which is susceptible to disruption upon transfer to new species. In this regard, it is
480 notable that the M segment splice donor and acceptor sites are identical between the human
481 and avian IAVs examined. M segment sequences outside of these canonical splice sites have,
482 however, been shown to modulate splicing efficiency [62-65]. Interestingly, $mRNA_7$ association
483 with mammalian SF2/ASF [64], and with mammalian hnRNPK and NS1-binding protein [65],
484 have been shown to alter the efficiency of splicing. Nucleotide differences in these binding
485 regions exist between human- and avian-adapted M segments. An interesting area of further
486 investigation will be to test whether there are differences in the binding of human and avian
487 $mRNA_7$ molecules to mammalian SF2/ASF, hnRNPK, and NS1-binding proteins.
488 The gene segments of IAVs circulating in humans are ultimately derived from the avian IAV
489 gene pool. Thus, the contrasting phenotypes conferred by avian- and human-adapted M
490 segments in mammalian cells suggest that a resetting of M segment gene expression to reduce
491 M2 levels has been positively selected following emergence of avian IAVs into mammalian
492 populations. Indeed, our data reveal that this adaptation has occurred in at least two

493 independent incidences: i) within the Eurasian avian-like swine lineage M, that emerged from
494 birds in the late 1970s and contributed the M segment to the pH1N1 virus prior to 2009; and ii)
495 within the human seasonal lineage derived from the 1918 pandemic, which contributed its M
496 segment to the H3N2 lineage represented by Pan99 virus. The timing of the adaptive changes
497 is unclear in each case and cannot be inferred from our data. Importantly, M2 expression in
498 human IAV mimics that of avian IAV in avian cells. Thus, restriction of splicing efficiency to
499 achieve low M2 levels appears to be an important feature of IAV host adaptation. Our data
500 furthermore suggest that the negative impact of an autophagy block on viral growth constitutes
501 an important pressure driving this selection.
502 To date, most publications related to autophagy in IAV-infected cells have used the PR8 or
503 WSN lab-adapted strains, the X31 variant of PR8, or avian IAVs [46,47,66,67]. We found that
504 PR8 virus expresses levels of M2 in mammalian cells that are comparable with avian IAVs. This
505 phenotype may be a result of adaptation to growth in chicken eggs. Owing to the use of viruses
506 carrying lab-adapted M segments, the current literature suggests that IAV infection routinely
507 induces a block in autophagy [46,47,66,67]. We also see evidence of such a block when using
508 viruses that express high levels of M2, but we propose that this phenotype is a symptom of poor
509 adaptation to the mammalian host cell. Analysis of viruses carrying human M segments in
510 mammalian cells suggests that low levels of M2 and activation, but not blocking, of autophagy
511 are the norm in IAV-infected cells.
512 While the previously reported block in autophagy induced by IAV has generally been interpreted
513 as a viral defense against an antiviral mechanism, a pro-viral role for autophagy is not without
514 precedent. In Dengue virus infection, autophagy has been reported to support viral replication.
515 Specifically, autophagic turnover of lipid droplets in infected cells is thought to provide energy
516 needed for viral growth and to supply phospholipids important during virion assembly [68-70].
517 For IAV, the availability of activated LC3B protein was reported to be important for viral
518 morphogenesis [46]. Specifically, M2 was implicated in recruitment of LC3B II to the plasma

519 membrane, and disruption of this recruitment was found to affect budding and reduce stability of
520 released virions [46]. We also noted strong redistribution of LC3B-GFP to the plasma
521 membrane during infection with viruses that express high levels of M2. This relocalization
522 occurred to a lesser extent in a well-matched IAV-host system (NL09 M in human cells), and
523 may play a functionally important role in this context. A role for LC3B II in morphogenesis is
524 consistent with the activation of autophagy having a pro-viral effect. Conversely, our data
525 indicate that a block in autophagic turnover reduces viral growth, potentially owing to disruption
526 of vesicular trafficking that is normally exploited by the virus [71-73], or due to disruption of
527 cellular metabolic functions on which the virus relies.
528 By inhibiting the proton channel activity of the avian M2 with amantadine, we found that a
529 functional channel is needed to bring about the observed effects on autophagy. Indeed, M2 has
530 been shown previously to block the fusion of autophagosomes with lysosomes in a proton
531 channel-dependent fashion [66]. Surprisingly, however, amantadine treatment was also found to
532 reduce LC3B II accumulation in PR8 NL09 M-infected cells. The pH1N1 M2 protein carries the
533 S31N mutation, which confers resistance to amantadine. Our data suggest that this resistance
534 is not effective at a relatively high concentration of 200 μM amantadine, at least in the context of
535 intracellular viral infection.
536 The mutagenesis of the M segment that we carried out with the goal of separating the effects of
537 M2 expression level from M2 amino acid sequence revealed an important constraint on M1
538 coding capacity. Namely, the human / avian amino acid polymorphisms introduced into the M1
539 ORF were found to impact regulation of M2 gene expression. Some or all of these non-
540 synonymous changes to M1 likely modulate the efficiency of $mRNA_7$ splicing. With this new
541 insight in mind, a fresh look at viral phenotypes previously attributed to M1 amino acid variations
542 is warranted. Effects of M1 amino acid sequence on virion morphology [25,31,32,74,75], for
543 example, may in fact be directly or indirectly mediated through changes in intracellular M2
544 expression level.

545 Notably, while an avian M2 protein was sufficient to support robust viral replication in
546 mammalian systems when expressed at low levels, this sufficiency did not extend to
547 transmission. Virus expressing the avian M2 from a human M segment transmitted poorly,
548 indicating that the IAV M2 carries viral determinants of transmission and that these determinants
549 are not well conserved between avian and human strains. This novel observation also supports
550 the notion that high replicative capacity of a virus in a given host species is not necessarily
551 sufficient for transmission between individuals. In this context, it will be interesting to evaluate
552 the impact of avian M2 amino acid signatures on virion stability in the environment.
553 In summary, our data suggest that adaptive change in the M segment is needed to maintain low
554 expression of M2 in mammalian cells and that, in the absence of such adaptive changes,
555 excess M2 limits viral growth by blocking the autophagy pathway. These findings establish
556 regulation of viral gene expression as a feature of the virus-host interface critical for IAV host
557 range determination and therefore emergence into novel host populations.
558

559 **Materials and Methods**

560 Ethics Statement

561 The Institutional Animal Care and Use Committee (IACUC) of Emory University approved the
562 study protocol under approval number PROTO201700595.
563

564 Cells

565 Madin-Darby Canine Kidney (MDCK) cells (a kind gift of Peter Palese, Icahn School of Medicine
566 at Mount Sinai) were maintained in minimal essential medium (Gibco) supplemented with 10%
567 fetal bovine serum (FBS) and penicillin-streptomycin. A549 and 293T cells were obtained from
568 the ATCC and maintained in Dulbecco's minimal essential medium (DMEM; Gibco)
569 supplemented with 10% FBS and penicillin-streptomycin. DF-1 cells were obtained from ATCC

570 and maintained in DMEM plus 5% FBS and penicillin-streptomycin. QT-6 cells were obtained
571 from ATCC and maintained in F-12K medium plus 5% FBS, 10% tryptose phosphate and
572 penicillin-streptomycin. All cells were incubated at 37°C with 5% CO_2.
573
574 Viruses
575 All viruses used in this work were generated using reverse genetics techniques [76]. The rescue
576 system for PR8 was a gift of Peter Palese (Icahn School of Medicine at Mount Sinai). The
577 rescue system for A/Panama/2007/99 (H3N2) [Pan/99] virus was initially described in [7]; and
578 that for A/Netherlands/602/2009 (H1N1) [NL09] virus was a gift of Ron Fouchier (Erasmus
579 Medical Center) [77]. The NL09 virus was propagated in MDCK cells for two passages. All other
580 virus stocks were generated in 10-11 day old embryonated chicken eggs.
581
582 Generation of chimeric M segments
583 Non-synonymous nucleotide changes differentiating NL09 and avian consensus M segments
584 were introduced in a reciprocal fashion into i) M1 and M2 to generate 16 mut viruses, ii) M1-only
585 to generate 9 mut viruses, and iii) M2-only to generate 7 mut viruses. The modified viral cDNAs
586 were synthesized by Genewiz and subcloned into the pDZ reverse genetic vector [78].
587
588 Sequence alignments and generation of consensus sequences
589 Alignment of the FASTA sequences downloaded from Genbank (or GISAID) databases was
590 carried out using DNASTAR Lasergene 13 MegAlign software running the Clustal W
591 phylogenetic alignment algorithm.
592 To obtain a consensus nucleotide sequence and to assess the degree of variability in the M
593 segment of H1N1 subtype avian IAVs, we searched the Genbank nucleotide database for full-
594 length M segment sequences derived from avian H1N1 subtype IAV collected between 1976
595 and 2008 from any temperate Northern hemisphere location. We obtained 262 sequences,

596 which included sequences with partial 3' and 5' UTRs, and manually curated the sequences to
597 (i) remove swine and human lineage derived H1N1 M segments, retaining 247 sequences, and
598 (ii) trim UTR sequences from the retained segments. Alignment of the sequences by Clustal W
599 provided a working consensus sequence and revealed up to 7% variability at the nucleotide
600 level among the selected avian host-derived sequences.
601 To assess the degree of amino acid variability in the M segment of avian IAV of any subtype, we
602 searched Genbank for full-length M1 or M2 protein sequences derived from avian H1Nx to
603 H16Nx subtype IAV, collected between 1970 and 2000, from any geographical location. These
604 dates were chosen to avoid selecting sequences representing isolates originating from the
605 repeated H5 subtype HPAI incursions into poultry populations which dominate the Genbank
606 database from the early 2000s onwards, and which would likely bias the subsequent analysis.
607 For each hemagglutinin subtype (H1Nx to H16Nx), we aligned the available sequences to
608 generate individual consensus M1 and M2 amino acid sequences (**Supplemental Table 1**), and
609 aligned those consensus sequences to the avian H1N1 subtype consensus M1 and M2
610 sequences, in order to assess amino acid diversity. The matrix proteins of each subtype, with
611 the exception of H9Nx, were 100% conserved. The H9Nx subtype matrix protein shared 97.6%
612 identity to the avian H1N1 sequence. The M2 proteins of each subtype were 100% conserved,
613 excepting H9Nx, H13Nx and H16Nx subtypes, which shared 97.2%, 94.8% and 93.8% identity
614 respectively, to the avian H1N1 consensus sequence. Thus, the amino acid composition of M1
615 and M2 proteins are highly conserved within wild waterfowl, particularly within isolates that
616 circulate among dabbling ducks and geese. In these host species, both M1 and M2 proteins are
617 at, or close to, 100% identity at the consensus amino acid level.
618 To identify a consensus nucleotide sequence for the 2009 pH1N1 IAV, and compare it to the
619 avian consensus sequence, we searched Genbank for full-length M segments derived from
620 pH1N1 subtype IAV isolated in North America, collected between the 7th June and the 20th June
621 2009, which was shortly after emergence of the pH1N1 lineage into the human population. 189

622 individual nucleotide sequences were obtained, curated, and aligned, to provide a working
623 consensus sequence for the pH1N1 M segment. The pH1N1 M segments possessed >2%
624 variability at the nucleotide level. The A/NL/602/09 (H1N1) (NL09) M segment is a 100% match
625 to the consensus sequence of the 2009 pH1N1 lineage at the nucleotide level, and the M
626 segment from this strain was adopted for use throughout the current study. Interestingly,
627 comparison of the NL09 M segment to the avian consensus sequence revealed 8.3% difference
628 at the nucleotide level, and 9 and 7 amino acid changes in M1 and M2 proteins, respectively
629 (**Table 2**). These data suggest that pH1N1 M segment possesses a nucleotide sequence that is
630 highly divergent from M segments obtained from viruses circulating within the wildfowl reservoir,
631 and which may encode host adaptive changes.
632
633 Evaluation of viral growth in cell culture
634 To assess growth, subconfluent cell monolayers in 6-well dishes were inoculated at an MOI of 5
635 PFU/cell (for single-cycle growth assays) or 0.01 PFU/cell (for multi-cycle growth assays) in a
636 200 µl volume. Following incubation for 1 h at 37°C, inocula were removed, cells washed 3x
637 with PBS and 2 ml viral growth medium (MEM (for MDCK cells), DMEM (for 293T, and DF1
638 cells), or F-12K (for A549, and QT-6 cells) medium plus 3% bovine serum albumin, penicillin
639 streptomycin, and TPCK-treated trypsin) was added. Infected cells were incubated at 37°C for
640 the remainder of the time-course. At the indicated time points, 120 µl medium was sampled from
641 each dish and 120 µl fresh medium was added to maintain a 2 ml volume. Samples were stored
642 at -80°C and later titered by plaque assay on MDCK cells. Each infection was performed in
643 triplicate and at least three biological replicate infections were carried out on different days. Data
644 are plotted as mean with SD and analyzed by repeated measures ANOVA.
645
646 Evaluation of viral growth in guinea pigs

647 Female, Hartley strain, guinea pigs weighing 300-350 g were obtained from Charles River
648 Laboratories. Prior to inoculation or nasal lavage, animals were sedated with a mixture of
649 ketamine (30 mg/kg) and xylazine (4 mg/kg). Virus used for inoculation was diluted in PBS to
650 allow intranasal inoculation of guinea pigs with $1x10^1$ to $1x10^3$ PFU in a 300 µl volume. Nasal
651 wash samples were collected as described previously [54], with PBS as the collection fluid.
652 Animals were housed in a Caron 6040 environmental chamber set to 10^oC and 20% RH
653 throughout the seven-day period and lids were left off of the cages during this time to ensure
654 environmental control within the cages [79].
655
656 Immunoblotting
657 A549 or DF-1 cells in 6-well plates were infected with the indicated IAVs and cells were lysed
658 with 2X Laemmli sample buffer (Bio-rad) plus 2% beta-mercaptoethanol at 8 hpi. Samples were
659 boiled at 95 ºC for 10 min and resolved on 4-20% gradient SDS-PAGE gels, followed by transfer
660 to nitrocellulose membranes (Bio-rad), and incubation of membranes with 5% non-fat dry
661 milk/TBST blocking buffer. Antibodies used for immunoblotting were: anti-vinculin monoclonal
662 antibody (catalog no. V9131; Sigma-Aldrich) at 1:5000 dilution, IAV nucleoprotein monoclonal
663 antibody (HT-103; catalog no. EMS010, Kerafast) at 1:1000 dilution, IAV matrix protein
664 monoclonal antibody (E10; catalog no. EMS009, Kerafast) at 1:1000 dilution, and LC3B
665 polyclonal antibody (Thermo Fisher Scientific) at 1:1000 dilution. Bands were quantified using
666 ImageLab software (Bio-rad) after normalization to vinculin. At least three biological replicate
667 viral infections were carried out, with two technical replicates of the immunoblotting for each
668 infection. Data shown with error bars representing SD and statistical analysis was carried out
669 using one-way ANOVA with Tukey's multiple comparisons in GraphPad Prism software.
670
671 RT primer extension assay

672 A549 or DF-1 cells in 6-well plates were infected with the specified IAVs and total RNA was
673 extracted 8 hpi using a RNeasy Kit (Qiagen). Total RNA was eluted in RNase-free water and
674 stored at -80 ºC until needed.
675 Radiolabeling of primers: 1 µmol of oligo DNA primer was incubated with 10 µCuries of [γ-
676 ^{32}P]ATP and 10 U of T4 PNK (New England Biolabs) in 70 mM Tris-HCl (pH 7.6) containing 10
677 mM $MgCl_2$ and 5 mM DTT. Radiolabeling reactions were carried out at 37 ºC for 1 h and diluted
678 to 30 µL with RNase-free water after termination of the reaction. Radiolabeled primers were
679 stored at –20 ºC until needed. 500 ng of total RNA was incubated with 0.45 µL unlabeled 5S
680 rRNA primer, 0.05 µL radiolabeled 5S rRNA primer, 0.25 µL radiolabeled IAV segment 7 vRNA
681 primer, and 0.25 µL radiolabeled IAV segment 7 mRNA primer in a final volume of 5 µL. Primers
682 were annealed to RNA by sequential incubations at 95 ºC for 3 min and ice for 3 min. Reactions
683 were pre-warmed at 50 ºC for 5 min. Transcription was initiated by the addition of 50 mM Tris-
684 HCl (pH 8.3) buffer containing 75 mM KCl, 3 mM MgCL2, 10 mM DTT, 2mM dNTP, and 50 units
685 of SuperScript III Reverse Transcriptase (Thermo Fisher Scientific). Reactions were incubated
686 at 50 ºC for 1 h and terminated by the addition of Gel Loading Buffer II (Thermo Fisher
687 Scientific) and incubation at 95 ºC for 10 min. Reactions were resolved on denaturing
688 sequencing polyacrylamide gels (7M urea, 6% acrylamide). Gels were subsequently dried and
689 exposed to a phosphor storage screen overnight. The intensity of bands was analyzed using a
690 Typhoon Trio Imager (GE Healthcare) and quantified with ImageQuant software (GE
691 Healthcare) after normalization to 5S rRNA. At least three biological replicate viral infections
692 were carried out, with two technical replicates of the RT primer extension assay for each
693 infection. Data are shown with error bars representing SD and statistical analysis was carried
694 out using one-way ANOVA with Tukey's multiple comparisons in GraphPad Prism software.
695
696 Fluorescence microscopy

697 To allow tracking of LC3B II and viral protein, cells grown on collagen-coated coverslips were
698 transduced with lentivirus expressing LC3B-GFP (BacMamm 2.0; catalog no. P36235,
699 ThermoFisher), as follows.
700 18h post-transduction, 293T or A549 cells were infected with the indicated IAVs at an MOI of 5
701 PFU/cell and incubated at 37°C. At 8h or 12 h post-IAV infection, cells were washed once with
702 PBS and fixed with 4% paraformaldehyde. Following permeabilization with 0.1% Triton X-100,
703 cells were incubated overnight at 4°C with anti-M2 monoclonal antibody (E10; catalog no.
704 EMS009, Kerafast). Three washes were performed prior to addition of goat anti-mouse Alexa
705 Fluor-647 secondary antibody (catalog no. A21241, Life Technologies) and incubation for 2 h at
706 room temperature. Antibody dilutions and washes were performed with PBS plus 1% Tween-20.
707 Cells were treated with DAPI, and coverslips were mounted on slides using Vectashield (Vector
708 Labs) mounting medium. Images were obtained with on a Nikon FV1000 confocal microscope at
709 the Emory Integrated Cellular Imaging core facility.
710
711 Drug treatments
712 Where indicated, chloroquine (Invitrogen) was added to cell culture medium at a final
713 concentration of 60 or 120 μM. Amantadine HCl (catalog no. 1018505, Sigma) was added to cell
714 culture medium at a final concentration of 200 μM. Both drugs were added to infected cells 1 h
715 after IAV inoculation.
716
717 Statistical analyses
718 Statistical analyses were performed in GraphPad Prism.
719 Multi-cycle and single-cycle growth in cell culture was assessed in three independent
720 experiments, with three technical sample replicates per experiment. Overall, statistical
721 significance was determined using repeated measures, two-way, multiple comparisons ANOVA
722 on log-transformed mean values, with Bonferroni correction applied to account for comparison

723 of a limited number of means, as well as by assessing pairwise comparisons of viruses at each
724 time point, except for single-cycle growth in cell culture in the presence of amantadine, which
725 was assessed in four independent experiments, with three technical sample replicates per
726 experiment. Overall statistical significance was determined using repeated measures, two-way,
727 multiple comparisons ANOVA on log-transformed values, with Sidak's correction applied, as
728 well as by assessing pairwise comparisons of viruses at each time point.
729
730 Growth of each virus in the guinea pig model was assessed in three independent experiments
731 with four guinea pigs per experiment. For transmission analysis, each guinea pig was treated as
732 an independent biological sample. Statistical significance in the magnitude of replication was
733 determined by comparing AUC of growth curves using two-tailed Student's t-test. Statistical
734 significance in transmission efficiency was determined using unpaired two-tailed Student's t-test.
735 Significance of differences in the kinetics of replication was determined by assessing the
736 interaction of time and virus using repeated measures, two-way ANOVA on mean log-
737 transformed values, with Bonferroni correction applied to account for comparison of a limited
738 number of means.
739 For experiments presented throughout the manuscript, unless specific values are provided, P
740 values are represented as follows: *< 0.05; **<0.01; ***< 0.001; ****< 0.0001.
741
742 **Acknowledgements**
743 We thank Paul Digard for his excellent advice relating to RT Primer Extension assays, and
744 Emory Integrated Cellular Imaging Core Facility for assistance with confocal imaging techniques.
745
746 **Figure Legends**
747 **Figure 1. pH1N1 M segment does not confer improved growth relative to avian M**
748 **segment in avian cells at 37°C. (A)** A panel of PR8-based viruses was rescued by reverse

749 genetics. The viruses differ only in the identity of the M segment, which were derived from
750 A/mallard/MN/99 (H3N8), A/rhea/NC/93 (H7N1), A/duck/Alberta/76 (H1N1), or A/NL/602/09
751 (H1N1) viruses. **(B)** 11-day-old embryonated chicken eggs (ECE) or (**C**) chicken DF-1 cells
752 were infected at low MOI with the indicated viruses. **(D)** Quail QT-6 cells or **(E)** DF-1 cells were
753 infected at a high MOI of 5 PFU/cell with the indicated viruses. In all avian systems assessed,
754 the pH1N1 M segment did not confer an increase in magnitude or kinetics of growth, relative to
755 any avian-origin M segment. Multi-cycle and single-cycle growth were assessed in three
756 independent experiments, with three technical replicates per experiment. Graphs show the
757 means with SD for the three experiments. Statistical significance was determined using
758 repeated measures, two-way, multiple ANOVA on log-transformed values, with Bonferroni
759 correction applied to account for comparison of a limited number of means.
760
761 **Figure 2. pH1N1 M segment confers higher growth relative to avian M segment in**
762 **mammalian cells at 37°C. (A)** Canine MDCK cells or **(B)** human A549 cells were inoculated
763 with the indicated viruses at a low MOI of 0.01 PFU/cell. **(C)** MDCK cells or **(D)** A549 cells were
764 inoculated with the indicated viruses at a high MOI of 5 PFU/cell. In mammalian cells, the
765 pH1N1 M segment conferred more rapid kinetics and higher peak titers than any avian-origin M
766 segment. Multi-cycle and single-cycle growth were assessed in three independent experiments,
767 with three technical sample replicates per experiment. Graphs show the means with SD for the
768 three experiments. Statistical significance was determined using repeated measures, two-way,
769 multiple ANOVA on log-transformed values, with Bonferroni correction applied to account for
770 comparison of a limited number of means. At each time point, pairwise comparisons between
771 viruses were performed, and asterisks corresponding to the most significant difference observed
772 is shown.
773

774 **Figure 3. pH1N1 influenza A virus M segment confers efficient replication and**
775 **transmission of PR8-based virus among guinea pigs.** Groups of four guinea pigs were
776 inoculated with 10 PFU of each avian M-encoding virus or NL09 M-encoding virus, as indicated.
777 **(A)** Virus replication in nasal wash was measured by plaque titration at days 2, 4, 6, and 8 post-
778 infection and the area under the curve was calculated. Graphs show mean AUC with SD for
779 three experiments. All avian M-encoding viruses exhibited lower levels of growth *in vivo* than the
780 isogenic virus possessing the NL09 M segment. The replication differences between avian M
781 and NL09 M-based viruses were statistically significant, whereas those among avian M-based
782 viruses were not. Statistical significance was evaluated using an unpaired, two-tailed Student's
783 t-test. **(B)** To assess transmission, each inoculated guinea pig was treated as an independent
784 biological sample. The pH1N1 M segment conferred efficient transmission to naïve animals that
785 were contact exposed (7/9 transmissions; 78%). In contrast, significantly poorer (12%), or no
786 transmission was observed from guinea pigs infected with PR8 avian M viruses to naïve cage
787 mates. Statistical significance of transmission differences were evaluated using an unpaired,
788 two-tailed Student's t-test.
789
790 **Figure 4. Ratio of M1 to M2 protein expression is high in DF-1 Cells irrespective of viral M**
791 **segment host origin.** DF-1 cells were inoculated at a MOI of 5 PFU/cell, with PR8 viruses
792 encoding avian or human-derived M segments, and incubated at 37°C for 8 h, then lysed.
793 Western immunoblot analysis of virus-infected DF-1 cells: **(A)** Vinculin expression was
794 measured to allow normalization of viral protein levels. NP expression was measured to assess
795 viral replication. Levels of M1 and M2 protein expression were assessed using an antibody
796 (Mab E10) to a common epitope at the amino terminus of M1 and M2 proteins, allowing relative
797 expression to be assessed. Levels of LC3B I and II were assessed using an antibody that
798 detects both the precursor and activated forms of LC3B protein. **(B)** M1 protein and **(C)** M2
799 protein were normalized to vinculin, quantitated and displayed as a percentage of total protein

800 expressed from the M gene. **(D)** The ratio of M1:M2 protein expression**. (E)** LC3B I protein and
801 **(F)** LC3B II protein were normalized, quantitated and displayed as a percentage of total LC3B
802 protein. Graphs in **B-F** show the means with SD from three independent experiments. For each
803 experiment, two replicate Western immunoblots were performed and quantitated. Statistical
804 significance was assessed using ordinary one-way ANOVA.
805
806 **Figure 5. High expression ratio of M1 to M2 protein in A549 cells is dependent upon viral**
807 **M segment host origin.** A549 cells were inoculated at a MOI of 5 PFU/cell with PR8 viruses
808 encoding avian or human-derived M segments and incubated at 37°C for 8 h, then lysed.
809 Western immunoblot analysis of virus-infected A549 cells: **(A)** Vinculin expression was
810 measured to allow normalization of viral protein levels. NP expression was measured to assess
811 viral replication. Levels of M1 and M2 protein expression were assessed using an antibody
812 (Mab E10) to a common epitope at the amino terminus of M1 and M2 proteins, allowing relative
813 expression to be assessed. Levels of LC3B I and II were assessed using an antibody that
814 detects both the precursor and activated forms of LC3B protein. **(B)** M1 protein and **(C)** M2
815 protein were normalized to vinculin, quantitated and displayed as a percentage of total protein
816 expressed from the M gene. **(D)** The ratio of M1:M2 protein expression. **(E)** LC3B I protein and
817 **(F)** LC3B II protein were normalized, quantitated and displayed as a percentage of total LC3B
818 protein. Graphs in **B-F** show the means with SD from three independent experiments. For each
819 experiment, two replicate Western immunoblots were performed and quantitated. Statistical
820 significance was assessed using ordinary one-way ANOVA.
821
822 **Figure 6. Ratio of mRNA$_7$ (encoding M1) to mRNA$_{10}$ (encoding M2) expression is high in**
823 **DF-1 cells irrespective of viral M Segment host origin.**
824 DF-1 cells were inoculated at a MOI of 5 PFU/cell with PR8 viruses encoding avian or human-
825 derived M segments and incubated at 37°C for 8 h prior to RNA extraction. RT primer extension

826 radiogram of virus-infected DF-1 cells: **(A)** 5S rRNA levels were measured to allow
827 normalization of viral RNA. Segment 7 vRNA expression was measured to assess viral
828 replication. Levels of $mRNA_7$, $mRNA_{10}$, and $mRNA_{11}$ mRNA expression were assessed using
829 radiolabeled probes. **(B)** $mRNA_7$, **(C)** $mRNA_{10}$, and **(D)** $mRNA_{11}$ was quantitated and displayed
830 as a percentage of total M gene-expressed mRNA. Graphs in **B-D** show the means with SD
831 from three independent experiments. For each experiment, two replicate radiograms were
832 quantitated. Statistical significance was assessed using ordinary one-way ANOVA.
833
834 **Figure 7. Ratio of $mRNA_7$ (encoding M1) to $mRNA_{10}$ (encoding M2) expression in A549**
835 **cells is dependent upon viral M segment host origin.** A549 cells were inoculated at a MOI of
836 5 PFU/cell with PR8 viruses encoding avian or human-derived M segments and incubated at
837 37°C for 8 h prior to RNA extraction. RT primer extension radiogram of virus-infected A549 cells:
838 **(A)** 5S rRNA levels were measured to allow normalization of viral RNA. Segment 7 vRNA
839 expression was measured to assess viral replication. Levels of $mRNA_7$, $mRNA_{10}$, and $mRNA_{11}$
840 mRNA expression were assessed using radiolabeled probes. **(B)** $mRNA_7$, **(C)** $mRNA_{10}$, and **(D)**
841 $mRNA_{11}$ was quantitated and displayed as a percentage of total M gene expressed mRNA.
842 Graphs in **B-D** show the means with SD from three independent experiments. For each
843 experiment, two replicate radiograms were quantitated. Statistical significance was assessed
844 using ordinary one-way ANOVA.
845
846 **Figure 8. In human cells, avian M2 was expressed at higher levels and localized more**
847 **strongly to perinuclear bodies than human M2.** A549 and 293T cells were inoculated with
848 the indicated viruses, encoding avian or human M segments, at a MOI of 5 PFU/cell. At 8 hpi
849 cells were stained with anti-M2 (Mab E10; red) and DAPI (blue) and imaged by confocal
850 microscopy. Examples of optical sections are shown, either as merged 2-color images or the
851 red and blue channels alone (shown in grey scale). **(A)** A549 cells with 63x optical and 3x digital

852 magnification (189x total magnification). **(B)** 293T cells with 63x optical and 3x digital
853 magnification (189x total magnification). Brightness was adjusted for optimal clarity, with all
854 images treated equally.
855
856 **Figure 9. Visualization of LC3 and M2 co-localization.**
857 293T cells were transduced with GFP-LC3 protein and inoculated 24 h later with the indicated
858 IAVs, encoding avian or human-derived M segments, at a MOI of 5 PFU/cell. Cells were fixed 8
859 h later and stained with anti-M2 (Mab E10; red) and DAPI (blue) followed by imaging with
860 confocal microscopy. CQ: chloroquine. Examples of optical sections are shown, either as
861 merged 3-color images, or the red, green, and blue channels alone (in grey scale). Images are
862 at 63x optical and 3x digital magnification (189x total magnification). Brightness was adjusted for
863 optimal clarity, with all images treated equally.
864
865 **Figure 10. Inhibition of M2 ion channel results in loss of activation of LC3B.**
866 A549 cells were inoculated at an MOI of 5 PFU/cell with PR8 viruses encoding avian or human-
867 derived M segments and incubated in the presence or absence of 200 μM amantadine from 1
868 hpi. Cells were lysed at 8 hpi. **(A)** Representative Western immunoblot. Vinculin expression was
869 measured to allow normalization of viral protein levels. NP expression was measured to assess
870 viral replication. Levels of M1 and M2 protein were assessed using an antibody (Mab E10) to a
871 common epitope of M1 and M2 proteins, allowing relative expression to be assessed. Levels of
872 LC3B I and II were assessed using an antibody that detects both the precursor and activated
873 forms of LC3B protein. **(B)** M1 protein and **(C)** M2 protein were normalized to vinculin and
874 displayed as a percentage of total M gene-expressed protein. **(D)** The ratio of M1:M2 protein
875 expression. **(E)** LC3B I and **(F)** LC3B II were normalized to vinculin and displayed as a
876 percentage of total LC3B protein. **(G)** As a control to ensure the specificity of amantadine, we
877 incubated chloroquine-treated A549 cells in the presence or absence of 200 μM amantadine for

878 8 h. **(H)** LC3B I and **(I)** LC3B II were normalized to vinculin and displayed as a percentage of
879 total LC3B protein. Graphs in **B-F, H-I** show the means with SD from three independent
880 experiments. For each experiment, two replicate Western immunoblots were performed and
881 quantitated. Statistical significance was assessed using ordinary one-way ANOVA.
882
883 **Figure 11. Inhibition of proton channel activity relieves M2-induced accumulation of**
884 **LC3B positive vesicles.** 293T cells transduced with LC3-GFP were inoculated at a MOI of 5
885 PFU/cell with PR8 viruses possessing M segments from a human or an avian strain and
886 incubated in the presence or absence of 200 μM amantadine from 1 hpi. Cells were fixed at 12
887 hpi and stained with anti-M2 (Mab E10; red) and DAPI (blue) followed by imaging with confocal
888 microscopy. Examples of optical sections are shown, either as merged 3-color images or the
889 red, green, and blue channels alone (in grey scale). 3x zoom of a 63x magnification is shown.
890 Brightness was adjusted for optimal clarity, with all images treated equally. CQ: chloroquine.
891
892 **Figure 12. Amantadine improves growth of avian M segment-encoding virus in A549 cells.**
893 PR8-based NL09 M or avian M-encoding viruses were inoculated at an MOI of 5 PFU/cell onto
894 A549 cells. At 1hpi, cells were treated with 200μM amantadine, and incubated at 37°C for 24 h
895 in the continuous presence of amantadine. Virus released into supernatant was collected at the
896 indicated time points, and virus growth was measured by plaque titration. The pH1N1 M
897 segment conferred more rapid kinetics and higher peak titers of growth than the avian-origin M
898 segment, however amantadine had no impact on the growth of the pH1N1 M encoding virus. In
899 contrast, growth of the avian M-encoding virus was improved in the presence of drug (P=
900 0.0007). Single-cycle growth was assessed in four independent experiments, with three
901 technical sample replicates per experiment. Graphs show the means with SD for the four
902 experiments. Statistical significance was determined using repeated measures, two-way,
903 multiple comparisons ANOVA on log-transformed values, with Sidak's correction applied.

904

905 **Figure 13. Activation of LC3B II correlates with high expression of M2 protein in A549**
906 **cells regardless of M2 amino acid composition.** PR8 NL09 M virus and PR8 avian M virus,
907 along with six chimeric variant PR8-based viruses, were inoculated at a MOI of 5 PFU/cell onto
908 A549 cells. Cells were incubated for 8 h, then lysed. **(A)** Western immunoblot analysis of virus-
909 infected A549 cells. Vinculin was measured to allow normalization of viral protein levels. NP was
910 measured to assess viral replication. Levels of M1 and M2 protein were assessed using an
911 antibody (Mab E10) to a common epitope at the amino terminus of M1 and M2 proteins,
912 allowing their direct comparison. Levels of LC3B I and II were assessed using an antibody that
913 detects both the precursor and activated forms of LC3B protein. **(B)** M1 protein and **(C)** M2
914 protein were normalized to vinculin and displayed as a percentage of total protein expressed
915 from the M gene. **(D)** The ratio of M1:M2 protein expression. **(E)** LC3B I protein and **(F)** LC3B II
916 protein were normalized to vinculin and displayed as a percentage of total LC3B protein. Graphs
917 in **B-F** show the means with SD from three independent experiments. For each experiment, two
918 replicate Western immunoblots were performed and quantitated. Statistical significance was
919 assessed using ordinary one-way ANOVA.

920

921 **Figure 14. pH1N1 M amino acid sequences are not sufficient to confer high growth**
922 **phenotype in A549 cells.** PR8 NL09 M virus and PR8 avian M virus, along with six PR8-based
923 viruses carrying avian-human chimeric M segments, were inoculated at a MOI of 5 PFU/cell
924 onto A549 cells. Virus growth was measured by plaque titration. The effects on viral growth of
925 amino acid changes in **(A)** both M1 and M2, **(B)** M1 only and **(C)** M2 only are shown. Single-
926 cycle growth was assessed in at least three independent experiments, with three technical
927 sample replicates per experiment. Graphed data show the means with SD for at least three
928 experiments. Statistical significance was determined using repeated measures, two-way,
929 multiple ANOVA on log-transformed values, with Bonferroni correction applied to account for

930 comparison of a limited no of means. Experiments involving PR8 NL09 9mut or 7mut viruses as
931 well as PR8 Av M 9mut or 7mut viruses were performed at the same time, but are displayed on
932 two separate graphs with the same PR8 NL09 M and PR8 avian M control virus data, to
933 improve clarity of presentation.
934
935 **Figure 15. Reduced expression of avian M2 improves replication efficiency *in vivo* but is**
936 **not sufficient for efficient transmission in guinea pigs.**
937 Groups of twelve guinea pigs were inoculated with 10 PFU of PR8-based viruses carrying avian
938 M, NL09 M, chimeric NL09 M 7mut M, or chimeric avian M 9mut segments, as indicated. **(A)**
939 Virus replication in nasal washings was measured by plaque titration at days 2, 4, 6, and 8 post-
940 infection and the total area under the curve was calculated. The replication differences between
941 viruses with NL09 M and NL09 M 7mutAv segments were not significant (P=0.720). Differences
942 between viruses encoding the NL09 M 7mut segment and the avian M 9mut segment trended
943 towards, but were not statistically significant (P=0.115). (**B**) Transmission to naïve cage mates
944 that were exposed at 24 hpi. Neither chimeric M segment conferred efficient transmission (7/9
945 transmissions; 78%). Statistical significance of replication differences was determined using a
946 two-tailed Student's t-test. Statistical significance of transmission differences was determined
947 using an unpaired two-tailed Student's t-test. NL M and avian M data are identical to data
948 presented in Figure 3 and are reproduced here for clarity.
949
950 **Figure 16. Regulation of M segment gene expression contributes to host range**
951 **restriction of IAV.** When an avian IAV M segment is transcribed within mammalian cells,
952 excessive splicing of $mRNA_7$ results in aberrant overexpression of the M2 proton channel. When
953 highly expressed, this channel accumulates in autophagic vesicles. Abundant proton channel
954 activity in the membranes of autophagosomes blocks their turnover by preventing fusion with
955 lysosomes. This stalling of a critical cellular housekeeping function in turn reduces the efficiency

956 of viral replication, contributing to the species barrier that limits the zoonotic potential of avian
957 IAVs.
958

959 **References**
960

961 1. Patterson KD, Pyle GF (1991) The geography and mortality of the 1918 influenza pandemic.
962 Bull Hist Med 65: 4-21.
963 2. Viboud C, Simonsen L, Fuentes R, Flores J, Miller MA, et al. (2016) Global Mortality Impact of
964 the 1957-1959 Influenza Pandemic. J Infect Dis 213: 738-745.
965 3. Viboud C, Grais RF, Lafont BA, Miller MA, Simonsen L, et al. (2005) Multinational impact of
966 the 1968 Hong Kong influenza pandemic: evidence for a smoldering pandemic. J Infect
967 Dis 192: 233-248.
968 4. Molinari NA, Ortega-Sanchez IR, Messonnier ML, Thompson WW, Wortley PM, et al. (2007)
969 The annual impact of seasonal influenza in the US: measuring disease burden and costs.
970 Vaccine 25: 5086-5096.
971 5. Reperant LA, Kuiken T, Osterhaus AD (2012) Adaptive pathways of zoonotic influenza viruses:
972 from exposure to establishment in humans. Vaccine 30: 4419-4434.
973 6. Lowen AC (2017) Constraints, Drivers, and Implications of Influenza A Virus Reassortment.
974 Annu Rev Virol.
975 7. Steel J, Lowen AC, Mubareka S, Palese P (2009) Transmission of influenza virus in a
976 mammalian host is increased by PB2 amino acids 627K or 627E/701N. PLoS Pathog 5:
977 e1000252.
978 8. Subbarao EK, London W, Murphy BR (1993) A single amino acid in the PB2 gene of influenza
979 A virus is a determinant of host range. J Virol 67: 1761-1764.
980 9. Linster M, van Boheemen S, de Graaf M, Schrauwen EJ, Lexmond P, et al. (2014)
981 Identification, characterization, and natural selection of mutations driving airborne
982 transmission of A/H5N1 virus. Cell 157: 329-339.
983 10. Long JS, Giotis ES, Moncorge O, Frise R, Mistry B, et al. (2016) Species difference in ANP32A
984 underlies influenza A virus polymerase host restriction. Nature 529: 101-104.
985 11. Rogers GN, Paulson JC (1983) Receptor determinants of human and animal influenza virus
986 isolates: differences in receptor specificity of the H3 hemagglutinin based on species of
987 origin. Virology 127: 361-373.
988 12. Tanner WD, Toth DJ, Gundlapalli AV (2015) The pandemic potential of avian influenza
989 A(H7N9) virus: a review. Epidemiol Infect 143: 3359-3374.
990 13. Capua I, Munoz O (2013) Emergence of influenza viruses with zoonotic potential: open
991 issues which need to be addressed. A review. Vet Microbiol 165: 7-12.
992 14. Cauldwell AV, Long JS, Moncorge O, Barclay WS (2014) Viral determinants of influenza A
993 host range. J Gen Virol.
994 15. Bosch FX, Hay AJ, Skehel JJ (1978) RNA and protein synthesis in a permissive and an abortive
995 influenza virus infection. In: Mahy BWJ, Barry RD, editors. Negative Strand Viruses and
996 the Host Cell. London, New York, San Francisco: Academic Press. pp. 465-474.
997 16. Valcavi PP, Conti G, Schito GC (1978) Macromolecular syntheses during abortive infection of
998 KB cells by influenza virus. In: Mahy BWJ, Barry RD, editors. Negative Strand Viruses and
999 the Host Cell. London, New York, San Francisco: Academic Press. pp. 475-482.
1000 17. Lohmeyer J, Talens LT, Klenk HD (1979) Biosynthesis of the influenza virus envelope in
1001 abortive infection. J Gen Virol 42: 73-88.

1002 18. Lamb RA, Lai CJ, Choppin PW (1981) Sequences of mRNAs derived from genome RNA
1003 segment 7 of influenza virus: colinear and interrupted mRNAs code for overlapping
1004 proteins. Proc Natl Acad Sci U S A 78: 4170-4174.
1005 19. Lamb RA, Choppin PW (1981) Identification of a second protein (M2) encoded by RNA
1006 segment 7 of influenza virus. Virology 112: 729-737.
1007 20. Inglis SC, Brown CM (1984) Differences in the control of virus mRNA splicing during
1008 permissive or abortive infection with influenza A (fowl plague) virus. J Gen Virol 65 (Pt
1009 1): 153-164.
1010 21. Lau SC, Scholtissek C (1995) Abortive infection of Vero cells by an influenza A virus (FPV).
1011 Virology 212: 225-231.
1012 22. Bogdanow B, Eichelbaum K, Sadewasser A, Wang X, Husic I, et al. (2018) The dynamic
1013 proteome of influenza A virus infection identifies M segment splicing as a host range
1014 determinant. BioRxiv: https://doi.org/10.1101/438176.
1015 23. Joseph U, Vijaykrishna D, Smith GJD, Su YCF (2018) Adaptive evolution during the
1016 establishment of European avian-like H1N1 influenza A virus in swine. Evol Appl 11: 534-
1017 546.
1018 24. Campbell PJ, Danzy S, Kyriakis CS, Deymier MJ, Lowen AC, et al. (2014) The M segment of
1019 the 2009 pandemic influenza virus confers increased NA activity, filamentous
1020 morphology and efficient contact transmissibility to A/Puerto Rico/8/1934-based
1021 reassortant viruses. J Virol.
1022 25. Campbell PJ, Kyriakis CS, Marshall N, Suppiah S, Seladi-Schulman J, et al. (2014) Residue 41
1023 of the Eurasian avian-like swine influenza a virus matrix protein modulates virion
1024 filament length and efficiency of contact transmission. J Virol 88: 7569-7577.
1025 26. Seladi-Schulman J, Steel J, Lowen AC (2013) Spherical Influenza Viruses Have a Fitness
1026 Advantage in Embryonated Eggs, while Filament-Producing Strains Are Selected In Vivo.
1027 J Virol 87: 13343-13353.
1028 27. Chou YY, Albrecht RA, Pica N, Lowen AC, Richt JA, et al. (2011) The M segment of the 2009
1029 new pandemic H1N1 influenza virus is critical for its high transmission efficiency in the
1030 guinea pig model. J Virol 85: 11235-11241.
1031 28. Lakdawala SS, Lamirande EW, Suguitan AL, Jr., Wang W, Santos CP, et al. (2011) Eurasian-
1032 origin gene segments contribute to the transmissibility, aerosol release, and
1033 morphology of the 2009 pandemic H1N1 influenza virus. PLoS Pathog 7: e1002443.
1034 29. Rossman JS, Lamb RA (2011) Influenza virus assembly and budding. Virology 411: 229-236.
1035 30. Pielak RM, Chou JJ (2010) Flu channel drug resistance: a tale of two sites. Protein Cell 1:
1036 246-258.
1037 31. Bourmakina SV, Garcia-Sastre A (2003) Reverse genetics studies on the filamentous
1038 morphology of influenza A virus. J Gen Virol 84: 517-527.
1039 32. Elleman CJ, Barclay WS (2004) The M1 matrix protein controls the filamentous phenotype of
1040 influenza A virus. Virology 321: 144-153.
1041 33. Stauffer S, Feng Y, Nebioglu F, Heilig R, Picotti P, et al. (2014) Stepwise priming by acidic pH
1042 and a high K+ concentration is required for efficient uncoating of influenza A virus cores
1043 after penetration. J Virol 88: 13029-13046.
1044 34. O'Neill RE, Talon J, Palese P (1998) The influenza virus NEP (NS2 protein) mediates the
1045 nuclear export of viral ribonucleoproteins. EMBO J 17: 288-296.

1046 35. Akarsu H, Burmeister WP, Petosa C, Petit I, Muller CW, et al. (2003) Crystal structure of the
1047 M1 protein-binding domain of the influenza A virus nuclear export protein (NEP/NS2).
1048 EMBO J 22: 4646-4655.
1049 36. Brunotte L, Flies J, Bolte H, Reuther P, Vreede F, et al. (2014) The nuclear export protein of
1050 H5N1 influenza A viruses recruits Matrix 1 (M1) protein to the viral ribonucleoprotein to
1051 mediate nuclear export. J Biol Chem 289: 20067-20077.
1052 37. Watanabe K, Handa H, Mizumoto K, Nagata K (1996) Mechanism for inhibition of influenza
1053 virus RNA polymerase activity by matrix protein. J Virol 70: 241-247.
1054 38. Zhang J, Pekosz A, Lamb RA (2000) Influenza virus assembly and lipid raft microdomains: a
1055 role for the cytoplasmic tails of the spike glycoproteins. J Virol 74: 4634-4644.
1056 39. Ali A, Avalos RT, Ponimaskin E, Nayak DP (2000) Influenza virus assembly: effect of influenza
1057 virus glycoproteins on the membrane association of M1 protein. J Virol 74: 8709-8719.
1058 40. Barman S, Adhikary L, Chakrabarti AK, Bernas C, Kawaoka Y, et al. (2004) Role of
1059 transmembrane domain and cytoplasmic tail amino acid sequences of influenza a virus
1060 neuraminidase in raft association and virus budding. J Virol 78: 5258-5269.
1061 41. Shimbo K, Brassard DL, Lamb RA, Pinto LH (1996) Ion selectivity and activation of the M2 ion
1062 channel of influenza virus. Biophys J 70: 1335-1346.
1063 42. Grambas S, Hay AJ (1992) Maturation of influenza A virus hemagglutinin--estimates of the
1064 pH encountered during transport and its regulation by the M2 protein. Virology 190: 11-
1065 18.
1066 43. Ciampor F, Thompson CA, Grambas S, Hay AJ (1992) Regulation of pH by the M2 protein of
1067 influenza A viruses. Virus Res 22: 247-258.
1068 44. Takeuchi K, Lamb RA (1994) Influenza virus M2 protein ion channel activity stabilizes the
1069 native form of fowl plague virus hemagglutinin during intracellular transport. J Virol 68:
1070 911-919.
1071 45. Rossman JS, Jing X, Leser GP, Lamb RA (2010) Influenza virus M2 protein mediates ESCRT-
1072 independent membrane scission. Cell 142: 902-913.
1073 46. Beale R, Wise H, Stuart A, Ravenhill BJ, Digard P, et al. (2014) A LC3-interacting motif in the
1074 influenza A virus M2 protein is required to subvert autophagy and maintain virion
1075 stability. Cell Host Microbe 15: 239-247.
1076 47. Gannage M, Dormann D, Albrecht R, Dengjel J, Torossi T, et al. (2009) Matrix protein 2 of
1077 influenza A virus blocks autophagosome fusion with lysosomes. Cell Host Microbe 6:
1078 367-380.
1079 48. Ren Y, Li C, Feng L, Pan W, Li L, et al. (2016) Proton Channel Activity of Influenza A Virus
1080 Matrix Protein 2 Contributes to Autophagy Arrest. J Virol 90: 591-598.
1081 49. Kovacs AL, Reith A, Seglen PO (1982) Accumulation of autophagosomes after inhibition of
1082 hepatocytic protein degradation by vinblastine, leupeptin or a lysosomotropic amine.
1083 Exp Cell Res 137: 191-201.
1084 50. Barr JN, Whelan SP, Wertz GW (1997) cis-Acting signals involved in termination of vesicular
1085 stomatitis virus mRNA synthesis include the conserved AUAC and the U7 signal for
1086 polyadenylation. J Virol 71: 8718-8725.
1087 51. Barr JN, Whelan SP, Wertz GW (1997) Role of the intergenic dinucleotide in vesicular
1088 stomatitis virus RNA transcription. J Virol 71: 1794-1801.

1089 52. Pagan I, Holmes EC, Simon-Loriere E (2012) Level of gene expression is a major determinant
1090 of protein evolution in the viral order Mononegavirales. J Virol 86: 5253-5263.
1091 53. Abraham G, Banerjee AK (1976) Sequential transcription of the genes of vesicular stomatitis
1092 virus. Proc Natl Acad Sci U S A 73: 1504-1508.
1093 54. Lowen AC, Mubareka S, Tumpey TM, Garcia-Sastre A, Palese P (2006) The guinea pig as a
1094 transmission model for human influenza viruses. Proc Natl Acad Sci U S A 103: 9988-
1095 9992.
1096 55. Lowen AC, Bouvier NM, Steel J (2014) Transmission in the guinea pig model. Curr Top
1097 Microbiol Immunol 385: 157-183.
1098 56. Inglis SC, Brown CM (1981) Spliced and unspliced RNAs encoded by virion RNA segment 7 of
1099 influenza virus. Nucleic Acids Res 9: 2727-2740.
1100 57. Fujita N, Itoh T, Omori H, Fukuda M, Noda T, et al. (2008) The Atg16L complex specifies the
1101 site of LC3 lipidation for membrane biogenesis in autophagy. Mol Biol Cell 19: 2092-
1102 2100.
1103 58. Hanada T, Noda NN, Satomi Y, Ichimura Y, Fujioka Y, et al. (2007) The Atg12-Atg5 conjugate
1104 has a novel E3-like activity for protein lipidation in autophagy. J Biol Chem 282: 37298-
1105 37302.
1106 59. Barth S, Glick D, Macleod KF (2010) Autophagy: assays and artifacts. J Pathol 221: 117-124.
1107 60. Mauthe M, Orhon I, Rocchi C, Zhou X, Luhr M, et al. (2018) Chloroquine inhibits autophagic
1108 flux by decreasing autophagosome-lysosome fusion. Autophagy 14: 1435-1455.
1109 61. Skehel JJ, Hay AJ, Armstrong JA (1978) On the mechanism of inhibition of influenza virus
1110 replication by amantadine hydrochloride. J Gen Virol 38: 97-110.
1111 62. van Wielink R, Harmsen MM, Martens DE, Peeters BP, Wijffels RH, et al. (2012) Mutations in
1112 the M-gene segment can substantially increase replication efficiency of NS1 deletion
1113 influenza A virus in MDCK cells. J Virol 86: 12341-12350.
1114 63. Spronken MI, van de Sandt CE, de Jongh EP, Vuong O, van der Vliet S, et al. (2017) A
1115 compensatory mutagenesis study of a conserved hairpin in the M gene segment of
1116 influenza A virus shows its role in virus replication. RNA Biol 14: 1606-1616.
1117 64. Shih SR, Krug RM (1996) Novel exploitation of a nuclear function by influenza virus: the
1118 cellular SF2/ASF splicing factor controls the amount of the essential viral M2 ion channel
1119 protein in infected cells. EMBO J 15: 5415-5427.
1120 65. Thompson MG, Munoz-Moreno R, Bhat P, Roytenberg R, Lindberg J, et al. (2018) Co-
1121 regulatory activity of hnRNP K and NS1-BP in influenza and human mRNA splicing. Nat
1122 Commun 9: 2407.
1123 66. Ren Y, Li C, Feng L, Pan W, Li L, et al. (2015) Proton Channel Activity of Influenza A Virus
1124 Matrix Protein 2 Contributes to Autophagy Arrest. J Virol 90: 591-598.
1125 67. Zhirnov OP, Klenk HD (2013) Influenza A virus proteins NS1 and hemagglutinin along with
1126 M2 are involved in stimulation of autophagy in infected cells. J Virol 87: 13107-13114.
1127 68. Heaton NS, Randall G (2011) Dengue virus and autophagy. Viruses 3: 1332-1341.
1128 69. Heaton NS, Randall G (2010) Dengue virus-induced autophagy regulates lipid metabolism.
1129 Cell Host Microbe 8: 422-432.
1130 70. Zhang J, Lan Y, Li MY, Lamers MM, Fusade-Boyer M, et al. (2018) Flaviviruses Exploit the
1131 Lipid Droplet Protein AUP1 to Trigger Lipophagy and Drive Virus Production. Cell Host
1132 Microbe 23: 819-831 e815.

1133 71. Henkel JR, Weisz OA (1998) Influenza virus M2 protein slows traffic along the secretory
1134 pathway. pH perturbation of acidified compartments affects early Golgi transport steps.
1135 J Biol Chem 273: 6518-6524.
1136 72. Henkel JR, Apodaca G, Altschuler Y, Hardy S, Weisz OA (1998) Selective perturbation of
1137 apical membrane traffic by expression of influenza M2, an acid-activated ion channel, in
1138 polarized madin-darby canine kidney cells. Mol Biol Cell 9: 2477-2490.
1139 73. Henkel JR, Popovich JL, Gibson GA, Watkins SC, Weisz OA (1999) Selective perturbation of
1140 early endosome and/or trans-Golgi network pH but not lysosome pH by dose-
1141 dependent expression of influenza M2 protein. J Biol Chem 274: 9854-9860.
1142 74. Burleigh LM, Calder LJ, Skehel JJ, Steinhauer DA (2005) Influenza a viruses with mutations in
1143 the m1 helix six domain display a wide variety of morphological phenotypes. J Virol 79:
1144 1262-1270.
1145 75. Roberts PC, Lamb RA, Compans RW (1998) The M1 and M2 proteins of influenza A virus are
1146 important determinants in filamentous particle formation. Virology 240: 127-137.
1147 76. Fodor E, Devenish L, Engelhardt OG, Palese P, Brownlee GG, et al. (1999) Rescue of
1148 influenza A virus from recombinant DNA. J Virol 73: 9679-9682.
1149 77. Chutinimitkul S, Herfst S, Steel J, Lowen AC, Ye J, et al. (2010) Virulence-Associated
1150 Substitution D222G in the Hemagglutinin of 2009 Pandemic Influenza A(H1N1) Virus
1151 Affects Receptor Binding. Journal of Virology 84: 11802-11813.
1152 78. Quinlivan M, Zamarin D, Garcia-Sastre A, Cullinane A, Chambers T, et al. (2005) Attenuation
1153 of equine influenza viruses through truncations of the NS1 protein. J Virol 79: 8431-8439.
1154 79. Lowen AC, Mubareka S, Steel J, Palese P (2007) Influenza virus transmission is dependent on
1155 relative humidity and temperature. PLoS Pathog 3: 1470-1476.
1156
1157
1158

1159 **Supporting Information Legends**

1160

1161 **Supplementary Figure 1. Schematic of M segment mRNAs and gene products.**

1162

1163 **(A)** The M segment of influenza virus is template for synthesis of $mRNA_7$ (encoding M1), mRNA
1164 M_{10} (encoding M2), and $mRNA_{11}$ (which encodes a putative but unconfirmed 10 amino acid
1165 peptide from a short open reading frame). (**B)** Pandemic H1N1 influenza virus M1 and M2
1166 proteins differ from the avian consensus sequences by 9 residues in M1 and 7 residues in M2.
1167 The M segments differ by 8.3% at the nucleotide level. (**C)** Seasonal H3N2 influenza virus strain
1168 A/Panama/2007/99 M1 and M2 proteins differ from the avian consensus sequences by 11

1169 residues in M1 and 14 residues in M2. The M segments differ by 9% at the nucleotide level. (**D)**
1170 Seasonal H3N2 influenza virus strain A/Bethesda/55/15 M1 and M2 proteins differ from the
1171 avian consensus sequences by 11 residues in M1 and 16 residues in M2. The M segments
1172 differ by 9.5% at the nucleotide level.
1173
1174 **Supplementary Figure 2. Human host-derived M segments confer higher growth to PR8-**
1175 **based viruses than avian host-derived M segments in mammalian cells at 37°C.**
1176
1177 PR8-based viruses were inoculated at a MOI of 5 PFU/cell onto human-derived 293T cells **(A)**,
1178 or A549 cells **(B)**. Cells were incubated at 37°C for up to 24 h. Virus released into supernatant
1179 was collected at the indicated time points, and virus growth was measured by plaque titration.
1180 Data obtained from viruses possessing human M segments are represented with blue lines:
1181 A/NL/602/09 M **(A,B)**, A/Panama/2007/99 M **(B)**, and A/Bethesda/15 M **(B)**, while data from
1182 viruses encoding avian M segments are represented with red lines. In each cell type, the human
1183 M segments conferred more rapid kinetics and higher peak titers of growth than any avian-origin
1184 M segment. Single-cycle growth was assessed in three independent experiments, with three
1185 technical sample replicates per experiment. Graphs show the means with SD for the three
1186 experiments. Statistical significance was determined using repeated measures, two-way,
1187 multiple ANOVA on log-transformed data, with Bonferroni correction applied as there were a
1188 limited no of means to compare.
1189
1190 **Supplementary Figure 3. pH1N1 influenza virus M segment increases kinetics of**
1191 **replication of PR8-based viruses among guinea pigs.**
1192
1193 Groups of four guinea pigs were inoculated with 10 PFU of each avian M-encoding virus, or
1194 NL09 M-encoding virus, as indicated. Graphs show individual titers obtained from animals used

1195 in three independent experiments. **(A-E)** Virus replication in nasal wash of inoculated animals
1196 was measured by plaque titration at days 2, 4, 6, and 8 post-infection and the titers at each time
1197 point were plotted (dotted lines). The differences between PR8 NL09 M and each avian M-
1198 encoding virus were considered significant. Statistical significance in kinetics of growth was
1199 determined by assessing the interaction of time and virus using repeated measures, two-way,
1200 multiple comparisons ANOVA on mean values, with Bonferroni correction applied to account for
1201 comparison of a limited no of means.
1202
1203 **Supplementary Figure 4. High expression ratio of M1 to M2 protein in human cells is**
1204 **dependent upon viral M segment host origin.**
1205
1206 293T and MDCK cells were inoculated at a MOI of 5 PFU/cell with PR8 viruses encoding avian
1207 or human-derived M segments and incubated at 37°C for 8 h, then cells were lysed. Western
1208 immunoblot analysis of virus-infected 293T cells **(A)** and MDCK cells **(G)**. Vinculin expression
1209 was measured to allow normalization of viral protein levels. NP expression was measured to
1210 assess viral replication. Levels of M1 and M2 protein expression were assessed using an
1211 antibody (Mab E10) to a common epitope at the amino terminus of M1 and M2 proteins,
1212 allowing relative expression to be assessed. Levels of LC3B I and II were assessed using an
1213 antibody that detects both the precursor and activated forms of LC3B protein. **(B, H)** M1 protein
1214 and **(C, I)** M2 protein were normalized to vinculin, quantitated and displayed as a percentage of
1215 total protein expressed from the M gene. **(D, J)** The ratio of M1:M2 protein expression. **(E, K)**
1216 LC3B I protein and **(F, L)** LC3BII protein were normalized, quantitated and displayed as a
1217 percentage of total LC3B protein. Graphs in **B-F**, and **H-K** show the means with SD from three
1218 independent experiments. For each experiment, two replicate Western immunoblots were
1219 performed and quantitated. Statistical significance was assessed using ordinary one-way
1220 ANOVA.

1221

1222

1223 **Supplementary Figure 5. High expression ratio of M1 to M2 protein in human cells is**

1224 **dependent upon viral M segment host origin.**

1225

1226 A549 cells were inoculated at a MOI of 5 PFU/cell with PR8 viruses encoding avian or human-

1227 derived M segments and incubated at 37°C for 8 h, then cells were lysed. Human M segments

1228 were derived from the following viruses: A/NL/602/09 (H1N1) (NL09); A/Panama/2007/99

1229 (H3N2) (Pan99); and A/Bethesda/15 (H3N2) (Beth15). Vinculin expression was measured to

1230 allow normalization of viral protein levels. NP expression was measured to assess viral

1231 replication. Levels of M1 and M2 protein expression were assessed using an antibody (Mab

1232 E10) to a common epitope at the amino terminus of M1 and M2 proteins, allowing relative

1233 expression to be assessed. Levels of LC3B I and II were assessed using an antibody that

1234 detects both the precursor and the activated forms of LC3B protein. Data presented are

1235 representative of Western immunoblots from three independent experiments.

1236

1237 **Supplementary Figure 6. Visualization of M2 localization by immunofluorescence**

1238 **microscopy at 12 h post-infection in A549 and 293T cells.**

1239

1240 A549 **(A, B)**, or 293T **(C, D)** cells were inoculated with the indicated viruses, encoding avian or

1241 human M segments, at a MOI of 5 PFU/cell. Cells were fixed at 12 hpi, permeabilised, and

1242 stained with anti-M2 (Mab E10; red) and DAPI (blue) followed by imaging with confocal

1243 microscopy. Examples of optical sections are shown, either as merged 2-color images or the

1244 red and blue channels alone (in grey scale). **(A)** A549 cells with 63x magnification. **(B)** 3x

1245 magnification of the same images shown in **A. (C)** 293T cells with 63x magnification. **(D)** 3x

1246 magnification of the same images shown in **C.** Brightness was adjusted for optimal clarity, with

1247 all images treated equally.

1248

1249 **Supplementary Figure 7. Visualization of LC3 and M2 co-localization by**

1250 **immunofluorescence microscopy.**

1251

1252 A549 cells were transduced with GFP-LC3 protein and inoculated 24 h later with the indicated

1253 IAVs, encoding avian- or human-derived M segments, at a MOI of 5 PFU/cell. Cells were fixed 8

1254 h later and stained with anti-M2 (Mab E10; red) and DAPI (blue) followed by imaging with

1255 confocal microscopy. Examples of optical sections are shown, either as merged 3-color images

1256 or the red, green, and blue channels alone (in grey scale). **(A)** 63x magnification. **(B)** 3x

1257 magnification of the same images shown in **A.** Brightness was adjusted for optimal clarity, with

1258 all images treated equally. CQ: chloroquine.

1259

1260 **Supplementary Figure 8. Chloroquine treatment results in loss of activation of LC3B.**

1261

1262 A549 cells were inoculated at a MOI of 5 PFU/cell with PR8 viruses encoding avian or human-

1263 derived M segments and incubated in the presence or absence of 60 μM chloroquine from 1 hpi.

1264 Cells were lysed with whole cell lysis buffer following 8 h incubation at 37°C. Western

1265 immunoblot of virus-infected A549 cells: **(A)** Vinculin expression was measured to allow

1266 normalization of viral protein levels. NP expression was measured to assess viral replication.

1267 Levels of M1 and M2 protein expression were assessed using an antibody (Mab E10) to a

1268 common epitope at the amino terminus of M1 and M2 proteins, allowing relative expression to

1269 be assessed. Levels of LC3B I and II were assessed using an antibody that detects both the

1270 precursor and the activated forms of LC3B protein. Data presented are representative Western

1271 immunoblots from three independent experiments. LC3B I protein and LC3B II protein **(B, C)**

1272 were normalized, quantitated and displayed as a percentage of total LC3B protein in the

1273 absence **(B)** or presence **(C)** of 60 μM chloroquine. Data presented in **B-C**, show the means
1274 with SD from three independent experiments. For each experiment, two replicate radiograms
1275 were quantitated. Statistical significance was assessed using ordinary two-way ANOVA. CQ:
1276 chloroquine.
1277
1278 **Supplementary Figure 9. Schematic depicting chimeric M Segment RNAs**
1279
1280 **(A)** Pandemic H1N1 influenza virus M1 and M2 proteins differ from the avian consensus
1281 sequences by 9 residues in M1 and 7 residues in M2. The pH1N1 amino acid identities are
1282 indicated in blue at their approximate positions within linear representations of M1 and M2
1283 proteins. The pH1N1 M segment differs from the avian consensus by 8.3% at the nucleotide
1284 level. Here, pH1N1 RNA sequence is indicated by blue coloring. **(B-D)** Chimeric human-avian M
1285 segments were constructed in which only the non-synonymous changes in the avian consensus
1286 were introduced into the A/NL/602/09 (H1N1) M segment. **(E)** Avian consensus M1 and M2
1287 proteins differ from the NL09 sequences by 9 residues in M1 and 7 residues in M2. The avian
1288 amino acid identities are indicated in red and avian RNA sequence is indicated by red coloring.
1289 **(F-H)** A second set of chimeric M segments was constructed in which the NL09 amino acid
1290 identities were introduced into the M segment of A/duck/Alberta/76 (H1N1) virus, yielding
1291 segments that encode avian consensus protein(s) but retain much of the nucleotide sequence
1292 of the NL09 M segment.
1293
1294 **Supplementary Figure 10. Visualization of LC3 and M2 co-localization in 293T cells**
1295 **infected with viruses carrying avian-human chimeric M segments.**
1296
1297 293T cells were transduced with GFP-LC3 protein and inoculated 24 h later with the indicated
1298 IAVs, encoding avian, human or chimeric M segments, at a MOI of 5 PFU/cell. Cells were fixed

1299 12 h later and stained with anti-M2 (Mab E10; red) and DAPI (blue) followed by imaging with
1300 confocal microscopy. Examples of optical sections are shown, either as merged 3-color images
1301 or the red, green, and blue channels alone (in grey scale). 3x magnification of 63x images are
1302 shown. Brightness was adjusted for optimal clarity, with all images treated equally.
1303
1304 **Supplementary Figure 11. Levels of $mRNA_7$ (encoding M1) and $mRNA_{10}$ (encoding M2)**
1305 **transcripts in A549 cells infected with viruses carrying human, avian or chimeric M**
1306 **segments.**
1307
1308 A549 cells were inoculated at a MOI of 5 PFU/cell with PR8 NL09 M virus and PR8 Av M virus,
1309 along with six PR8-based viruses with chimeric M segments. Cells were incubated at 37°C for 8
1310 h and then lysed with a RNeasy Kit. **(A)** RT primer extension radiogram of virus-infected A549
1311 cells. 5S rRNA levels were measured to allow normalization of viral RNA. Segment 7 vRNA
1312 expression was measured to assess viral replication. **(B)** Levels of $mRNA_7$, **(C)** $mRNA_{10}$, and
1313 **(D)** $mRNA_{11}$ were quantitated and displayed as a percentage of total M gene expressed mRNA.
1314 Graphs in **B-D** show the means with SD from three independent experiments. For each
1315 experiment, two replicate radiograms were quantitated. Statistical significance was assessed
1316 using ordinary one-way ANOVA.
1317
1318 **Supplementary Figure 12. High expression of M2 protein reduces kinetics of replication**
1319 **of PR8-based viruses in guinea pigs.**
1320
1321 Groups of four guinea pigs were inoculated with 10 PFU of each chimeric M-encoding virus, as
1322 indicated. Graphs show individual titers obtained from animals used in three independent
1323 experiments. Virus replication in nasal wash of inoculated animals was measured by plaque
1324 titration at days 2, 4, 6, and 8 post-infection and the titers at each time point were plotted (dotted

1325 lines). The differences between PR8 NL09 M 7 mut Av and avian M 9 mut NL encoding viruses
1326 were considered significant. Statistical significance in kinetics of growth was determined by
1327 assessing the interaction of time and virus using repeated measures, two-way, multiple
1328 comparisons ANOVA on mean values, with Bonferroni correction applied to account for
1329 comparison of a limited no of means.
1330
1331 **Supplementary Figure 13. PR8 M2 protein is overexpressed and partly localized in**
1332 **perinuclear vesicles in 293T cells.**
1333
1334 293T cells were inoculated with the indicated IAVs, encoding avian-, human- or PR8-derived M
1335 segments, at a MOI of 5 PFU/cell, or treated with 60 μM chloroquine. Cells were fixed 8 h later
1336 and stained with anti-M2 (Mab E10; red) and DAPI (blue) followed by imaging with confocal
1337 microscopy. Examples of optical sections are shown, either as merged 2-color images or the
1338 red and blue channels alone (in grey scale). 63x magnification with 3x optical zoom. Brightness
1339 was adjusted for optimal clarity, with all images treated equally. CQ: chloroquine.

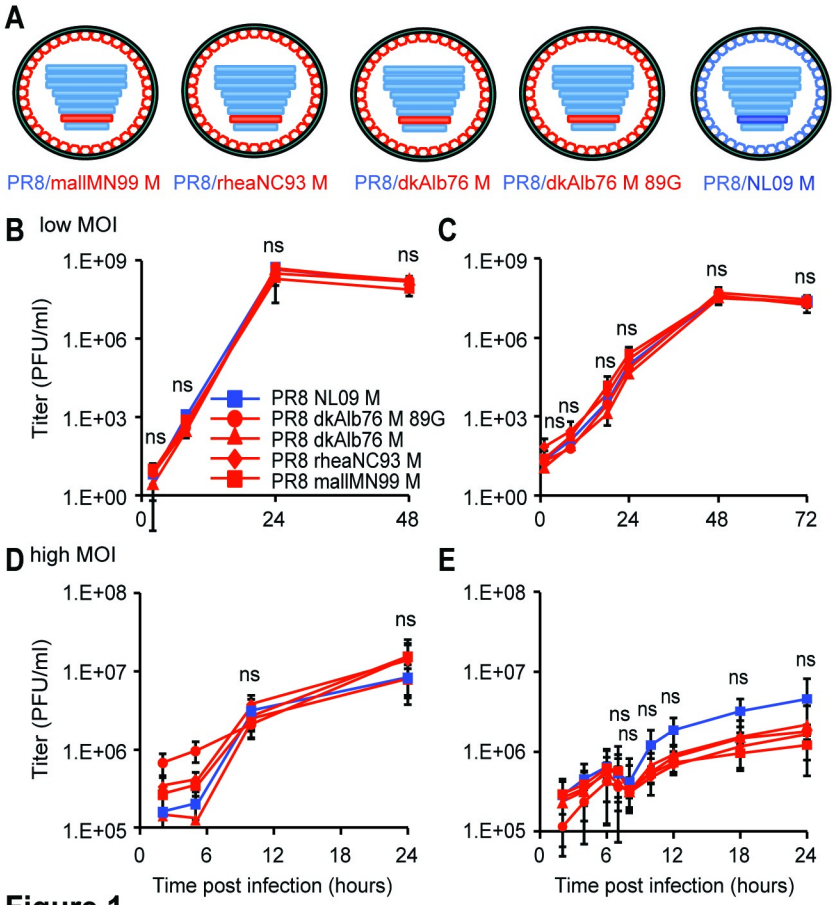
A
PR8/mallMN99 M
PR8/rheaNC93 M
PR8/dkAlb76 M
PR8/dkAlb76 M 89G
PR8/NL09 M
B low MOI
C
D high MOI
E
Titer (PFU/ml)
Time post infection (hours)
PR8 NL09 M
PR8 dkAlb76 M 89G
PR8 dkAlb76 M
PR8 rheaNC93 M
PR8 mallMN99 M
ns

Figure 1

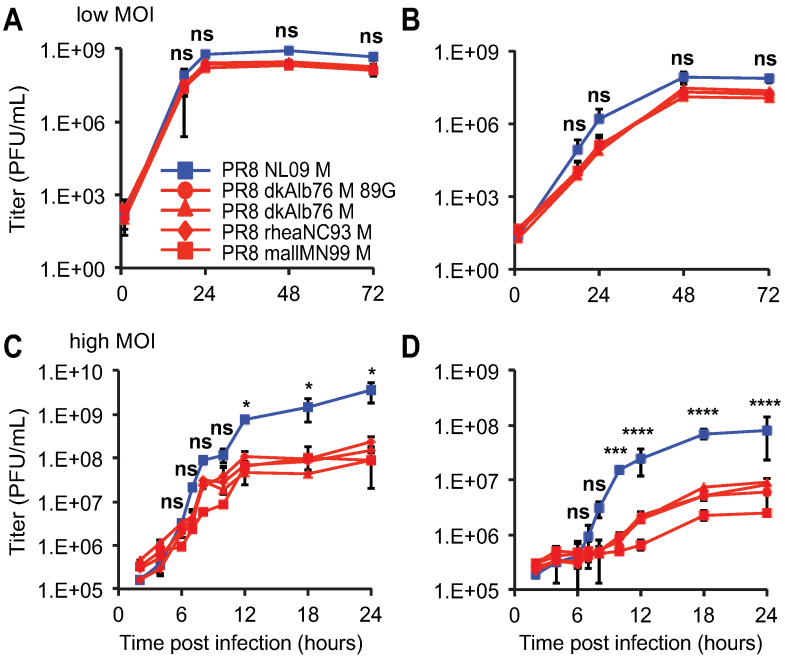
A
low MOI
B
C
high MOI
D
Titer (PFU/mL)
Time post infection (hours)
PR8 NL09 M
PR8 dkAlb76 M 89G
PR8 dkAlb76 M
PR8 rheaNC93 M
PR8 mallMN99 M
ns
*
***
****

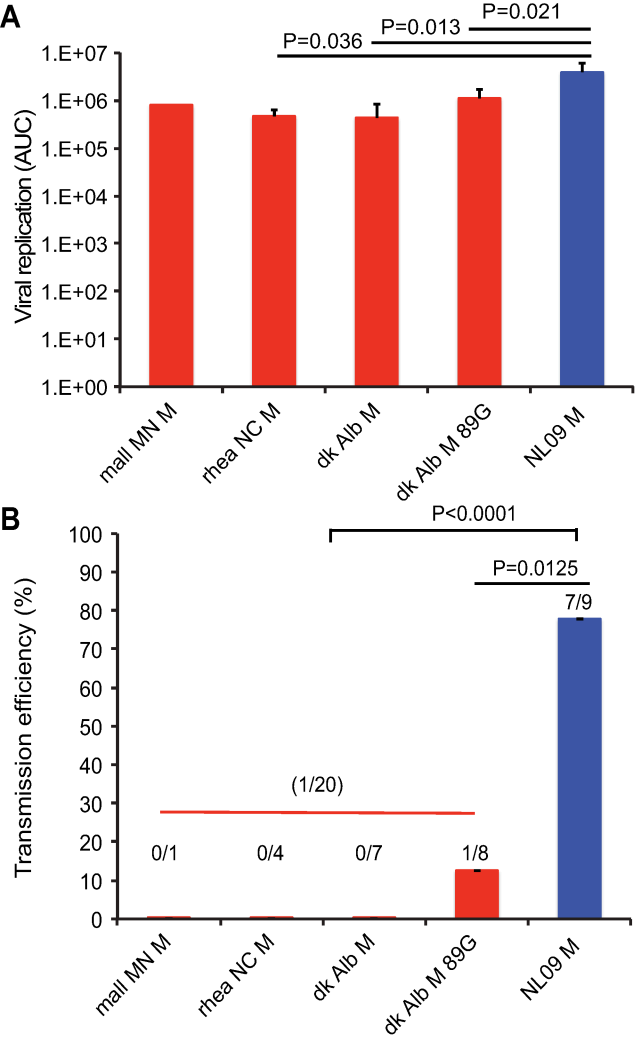
A
P=0.036
P=0.013
P=0.021
Viral replication (AUC)
1.E+07
1.E+06
1.E+05
1.E+04
1.E+03
1.E+02
1.E+01
1.E+00
mall MN M
rhea NC M
dk Alb M
dk Alb M 89G
NL09 M
B
P<0.0001
P=0.0125
Transmission efficiency (%)
100
90
80
70
60
50
40
30
20
10
0
7/9
(1/20)
0/1
0/4
0/7
1/8
mall MN M
rhea NC M
dk Alb M
dk Alb M 89G
NL09 M

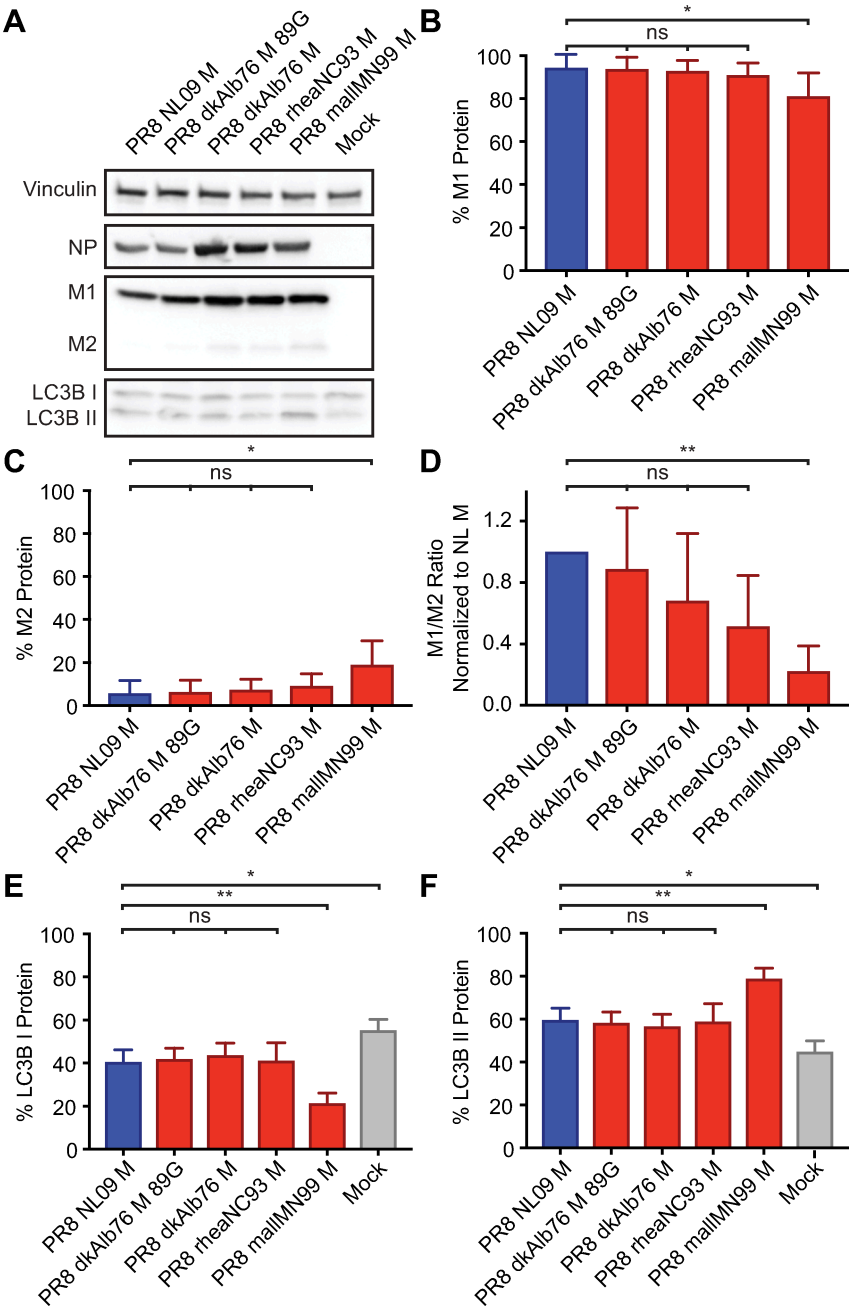
A
PR8 NL09 M
PR8 dkAlb76 M 89G
PR8 dkAlb76 M
PR8 rheaNC93 M
PR8 malIMN99 M
Mock
Vinculin
NP
M1
M2
LC3B I
LC3B II
B
% M1 Protein
ns
*
C
% M2 Protein
D
M1/M2 Ratio
Normalized to NL M
**
E
% LC3B I Protein
F
% LC3B II Protein

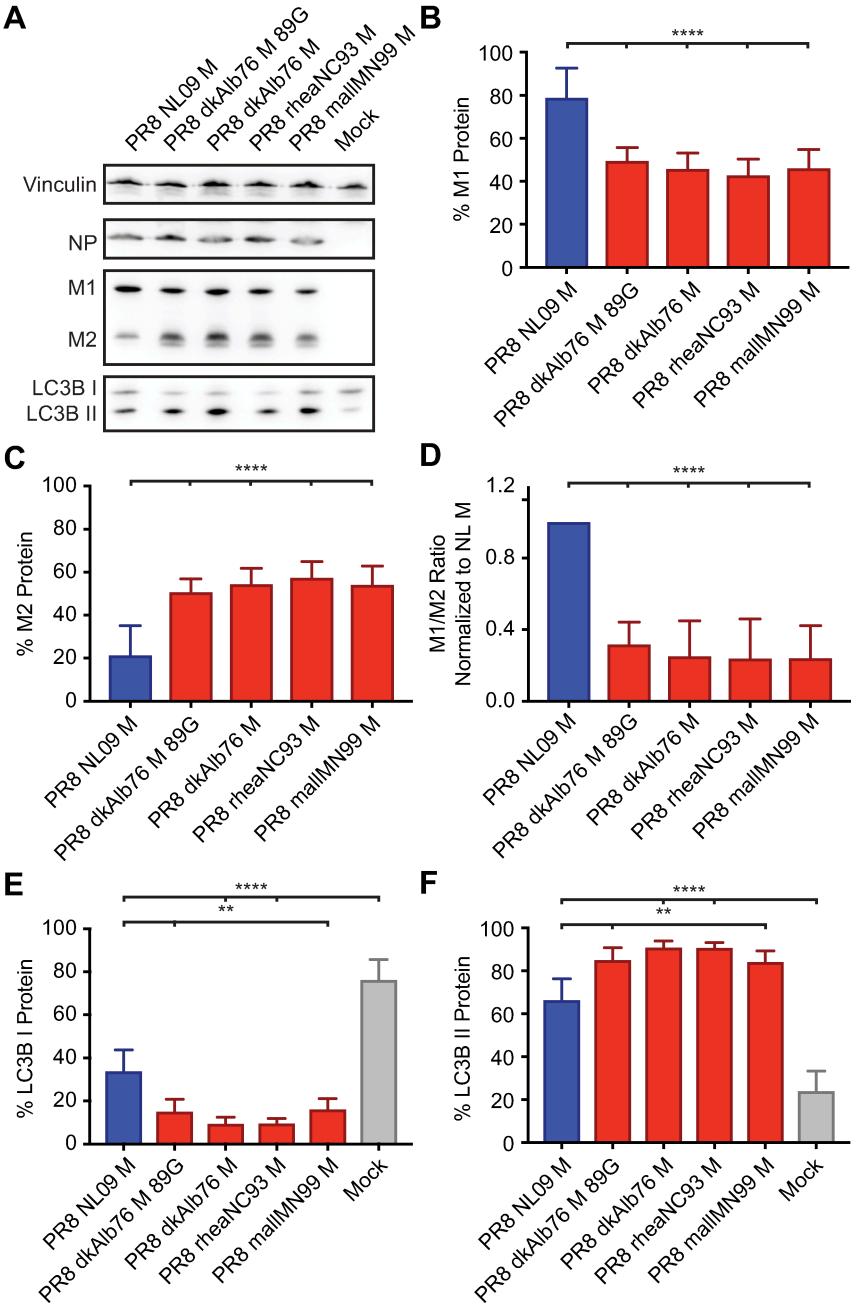
A
PR8 NL09 M
PR8 dkAlb76 M 89G
PR8 dkAlb76 M
PR8 rheaNC93 M
PR8 malIMN99 M
Mock
Vinculin
NP
M1
M2
LC3B I
LC3B II
B
% M1 Protein
****
C
% M2 Protein
****
D
M1/M2 Ratio
Normalized to NL M
****
E
% LC3B I Protein
****
**
F
% LC3B II Protein
****
**

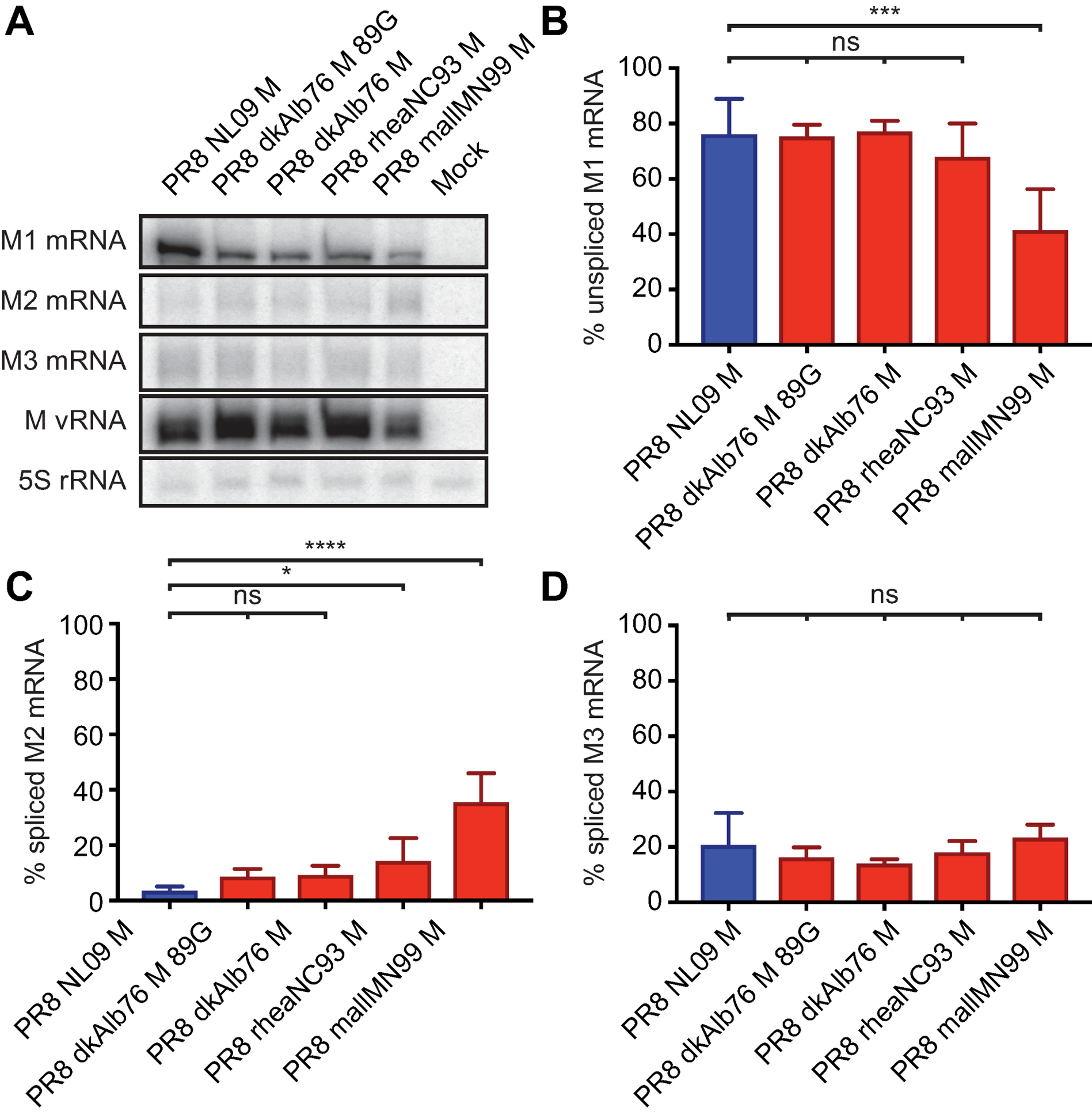
A
PR8 NL09 M
PR8 dkAlb76 M 89G
PR8 dkAlb76 M
PR8 rheaNC93 M
PR8 mallMN99 M
Mock
M1 mRNA
M2 mRNA
M3 mRNA
M vRNA
5S rRNA
B
***
ns
% unspliced M1 mRNA
100
80
60
40
20
0
PR8 NL09 M
PR8 dkAlb76 M 89G
PR8 dkAlb76 M
PR8 rheaNC93 M
PR8 mallMN99 M
C
****
*
ns
% spliced M2 mRNA
100
80
60
40
20
0
PR8 NL09 M
PR8 dkAlb76 M 89G
PR8 dkAlb76 M
PR8 rheaNC93 M
PR8 mallMN99 M
D
ns
% spliced M3 mRNA
100
80
60
40
20
0
PR8 NL09 M
PR8 dkAlb76 M 89G
PR8 dkAlb76 M
PR8 rheaNC93 M
PR8 mallMN99 M

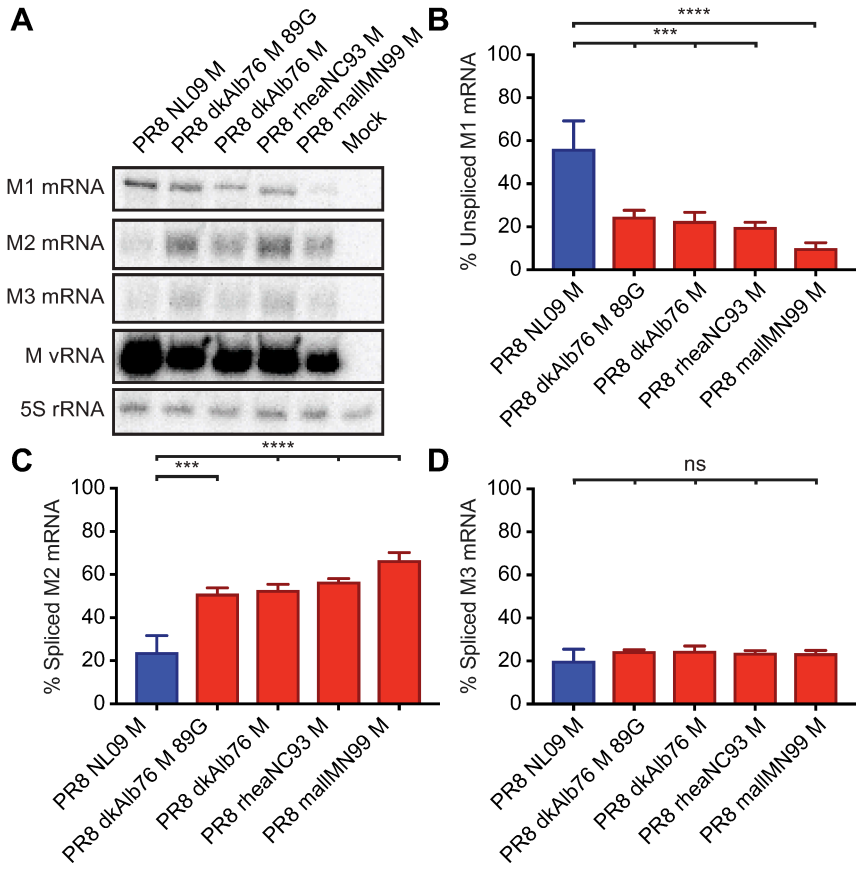
A
PR8 NL09 M
PR8 dkAlb76 M 89G
PR8 dkAlb76 M
PR8 rheaNC93 M
PR8 mallMN99 M
Mock
M1 mRNA
M2 mRNA
M3 mRNA
M vRNA
5S rRNA
B
****
***
% Unspliced M1 mRNA
100
80
60
40
20
0
PR8 NL09 M
PR8 dkAlb76 M 89G
PR8 dkAlb76 M
PR8 rheaNC93 M
PR8 mallMN99 M
C
****
***
% Spliced M2 mRNA
100
80
60
40
20
0
PR8 NL09 M
PR8 dkAlb76 M 89G
PR8 dkAlb76 M
PR8 rheaNC93 M
PR8 mallMN99 M
D
ns
% Spliced M3 mRNA
100
80
60
40
20
0
PR8 NL09 M
PR8 dkAlb76 M 89G
PR8 dkAlb76 M
PR8 rheaNC93 M
PR8 mallMN99 M

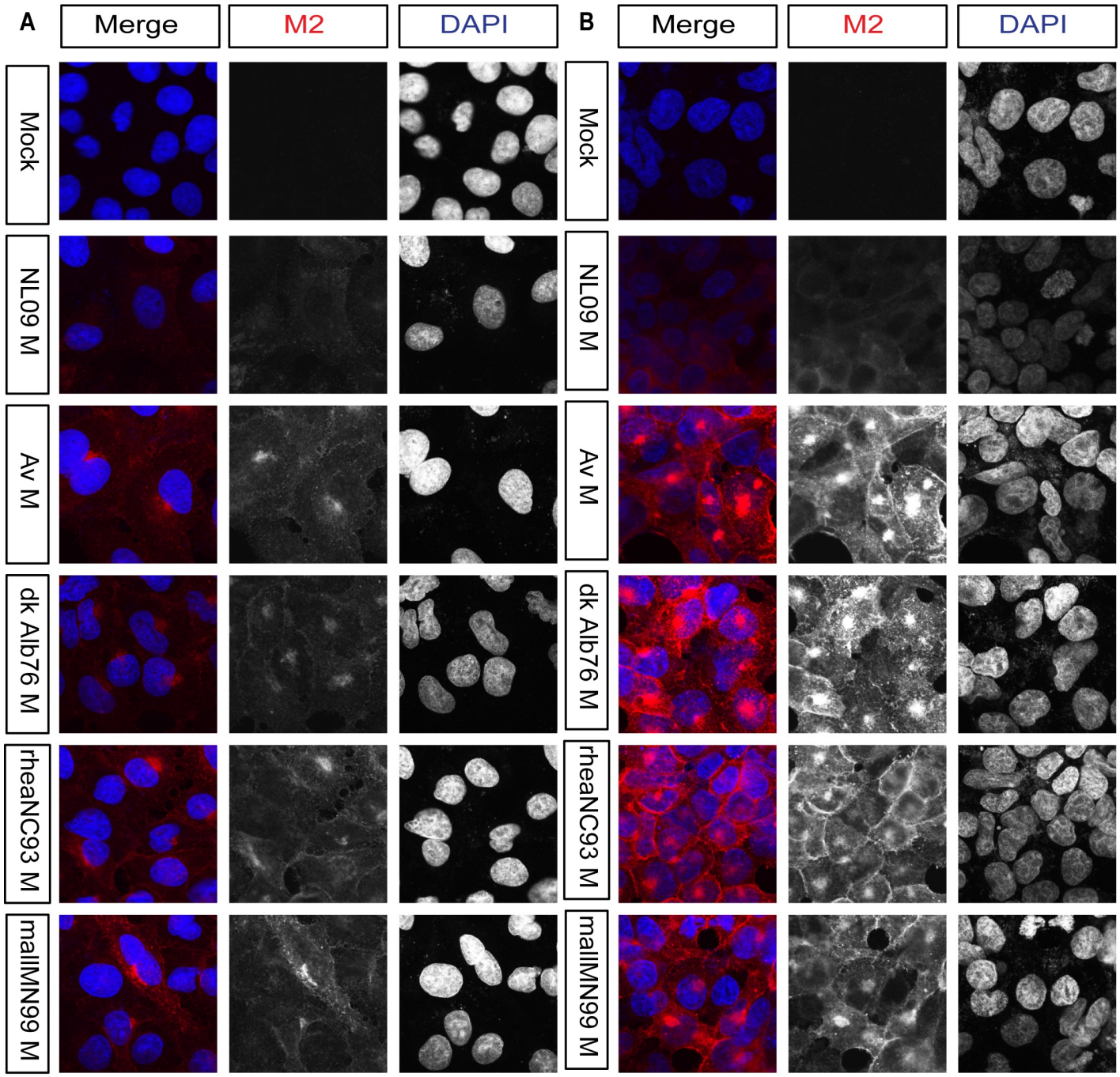
A
Merge
M2
DAPI
Mock
NL09 M
Av M
dk Alb76 M
rheaNC93 M
mallMN99 M
B
Merge
M2
DAPI
Mock
NL09 M
Av M
dk Alb76 M
rheaNC93 M
mallMN99 M

Figure 8

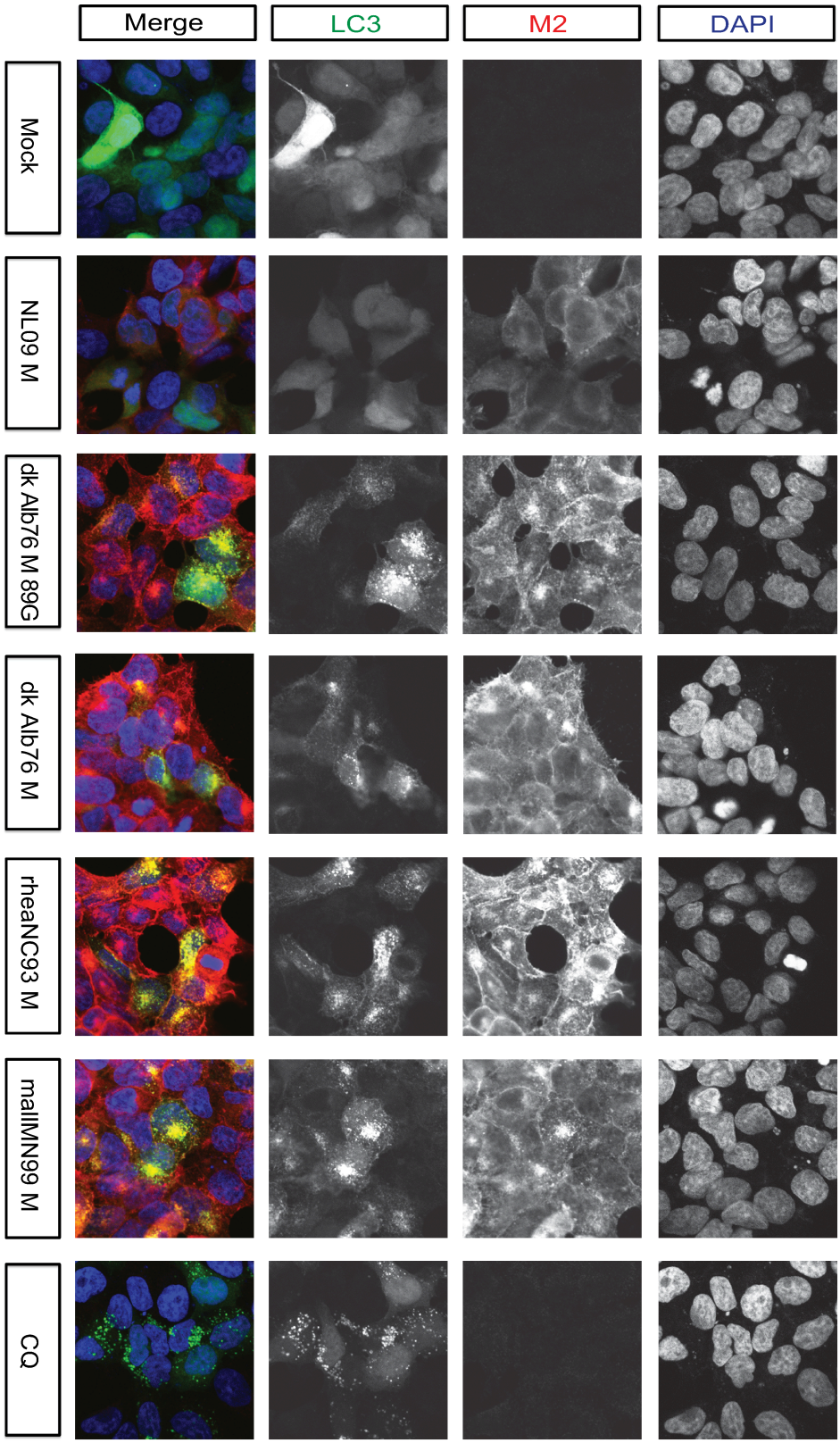
Merge
LC3
M2
DAPI
Mock
NL09 M
dk Alb76 M 89G
dk Alb76 M
rheaNC93 M
mallMN99 M
CQ

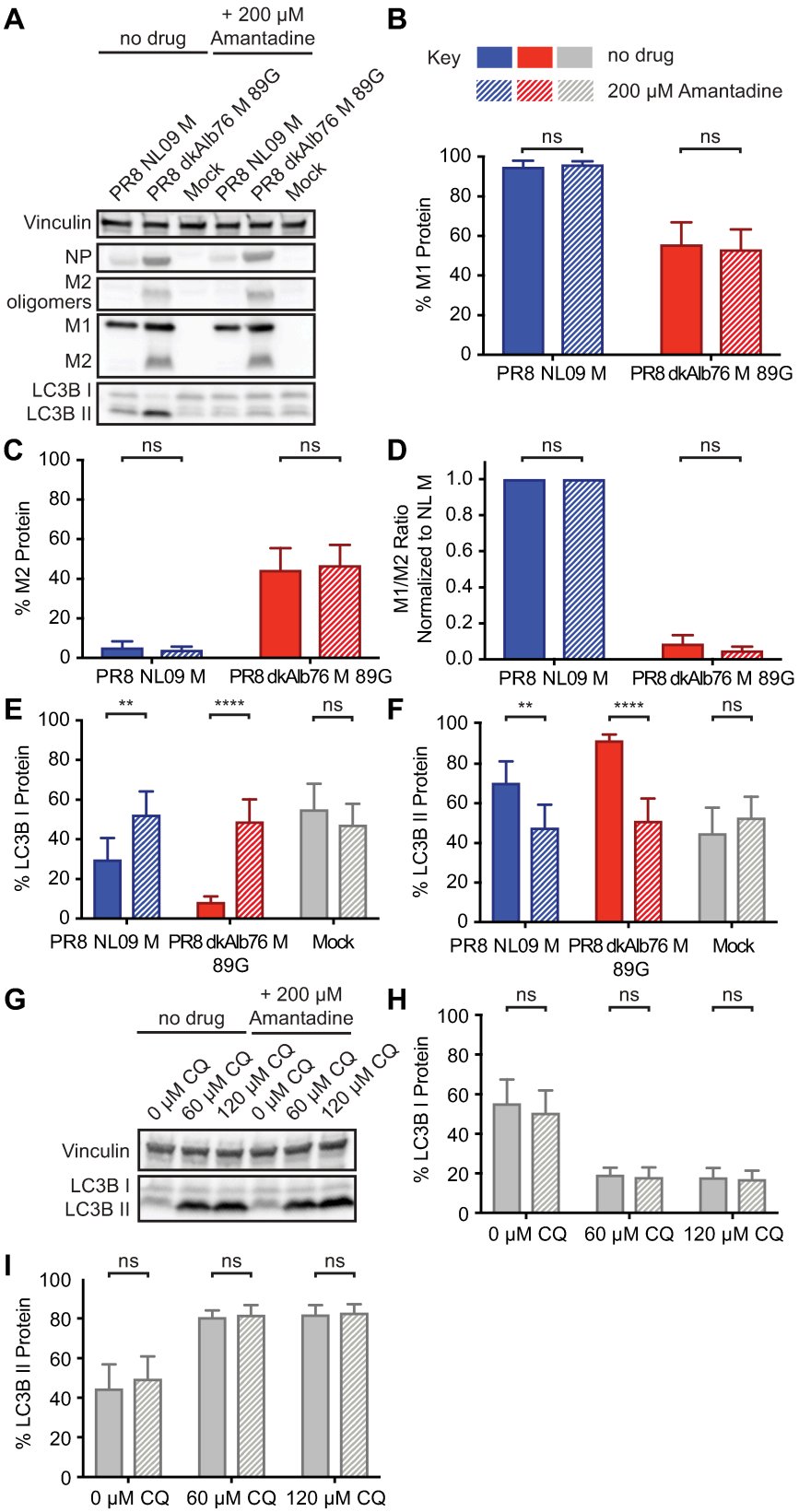
A
no drug
+ 200 μM Amantadine
PR8 NL09 M
PR8 dkAlb76 M 89G
Mock
PR8 NL09 M
PR8 dkAlb76 M 89G
Mock
Vinculin
NP
M2 oligomers
M1
M2
LC3B I
LC3B II
B
Key
no drug
200 μM Amantadine
ns
ns
% M1 Protein
100
80
60
40
20
0
PR8 NL09 M
PR8 dkAlb76 M 89G
C
ns
ns
% M2 Protein
100
80
60
40
20
0
PR8 NL09 M
PR8 dkAlb76 M 89G
D
ns
ns
M1/M2 Ratio Normalized to NL M
1.0
0.8
0.6
0.4
0.2
0.0
PR8 NL09 M
PR8 dkAlb76 M 89G
E
**
****
ns
% LC3B I Protein
100
80
60
40
20
0
PR8 NL09 M
PR8 dkAlb76 M 89G
Mock
F
**
****
ns
% LC3B II Protein
100
80
60
40
20
0
PR8 NL09 M
PR8 dkAlb76 M 89G
Mock
G
no drug
+ 200 μM Amantadine
0 μM CQ
60 μM CQ
120 μM CQ
0 μM CQ
60 μM CQ
120 μM CQ
Vinculin
LC3B I
LC3B II
H
ns
ns
ns
% LC3B I Protein
100
80
60
40
20
0
0 μM CQ
60 μM CQ
120 μM CQ
I
ns
ns
ns
% LC3B II Protein
100
80
60
40
20
0
0 μM CQ
60 μM CQ
120 μM CQ

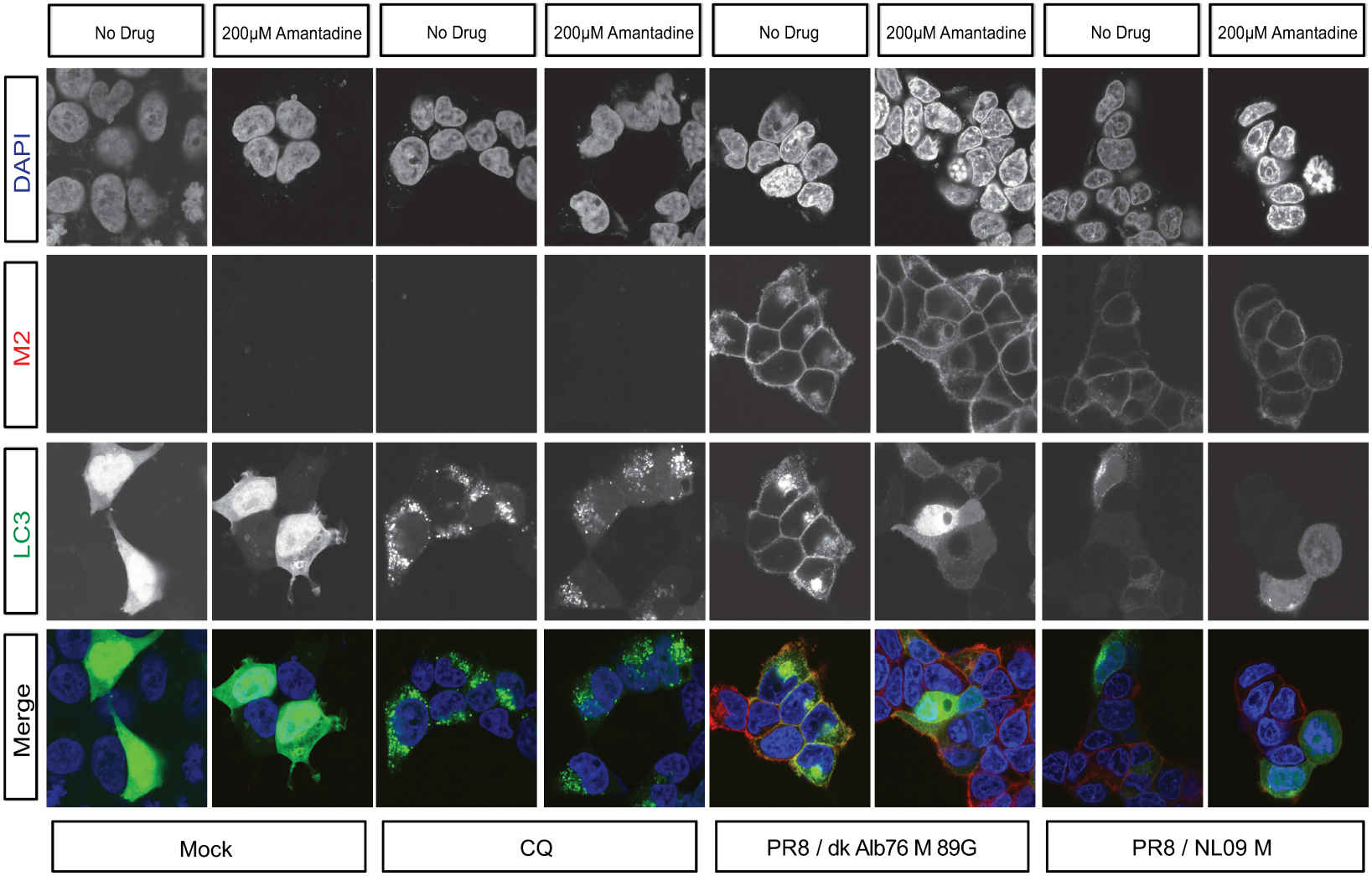
No Drug
200μM Amantadine
No Drug
200μM Amantadine
No Drug
200μM Amantadine
No Drug
200μM Amantadine
DAPI
M2
LC3
Merge
Mock
CQ
PR8 / dk Alb76 M 89G
PR8 / NL09 M

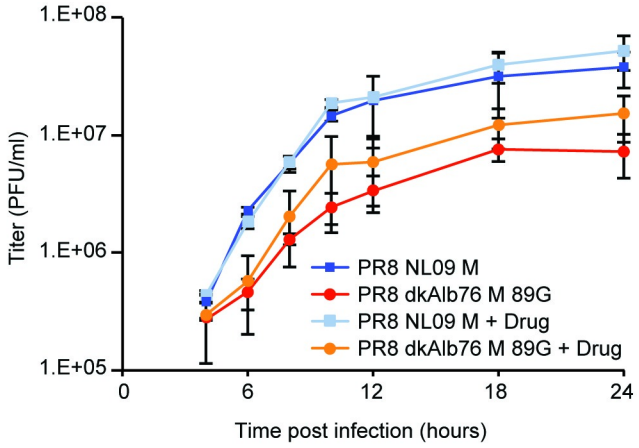
1.E+08
1.E+07
1.E+06
1.E+05
Titer (PFU/ml)
0
6
12
18
24
Time post infection (hours)
PR8 NL09 M
PR8 dkAlb76 M 89G
PR8 NL09 M + Drug
PR8 dkAlb76 M 89G + Drug

Figure 12

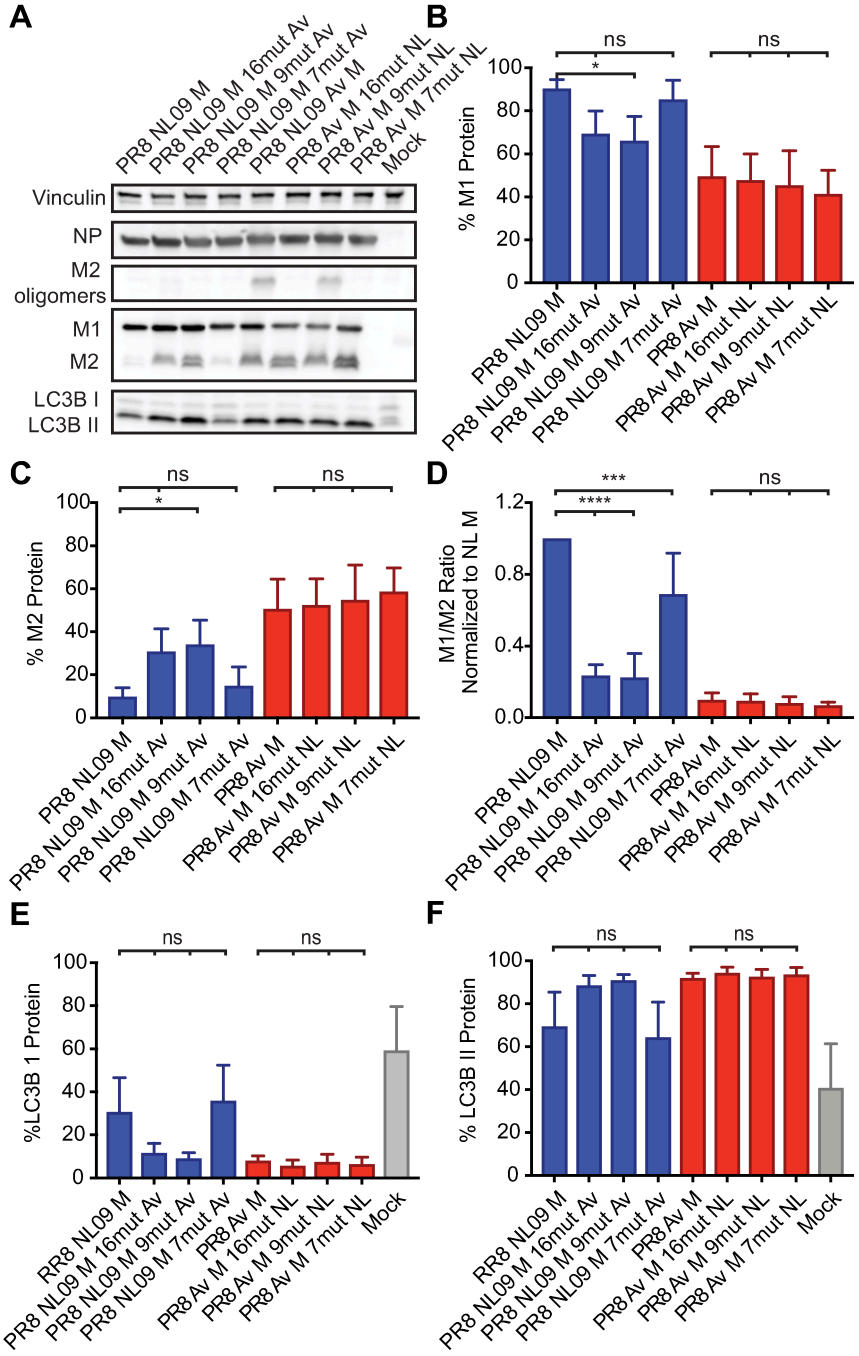
A
PR8 NL09 M
PR8 NL09 M 16mut Av
PR8 NL09 M 9mut Av
PR8 NL09 M 7mut Av
PR8 NL09 Av M
PR8 Av M 16mut NL
PR8 Av M 9mut NL
PR8 Av M 7mut NL
Mock
Vinculin
NP
M2 oligomers
M1
M2
LC3B I
LC3B II
B
% M1 Protein
ns
*
ns
C
% M2 Protein
ns
*
ns
D
M1/M2 Ratio Normalized to NL M
***
****
ns
E
%LC3B 1 Protein
ns
ns
F
% LC3B II Protein
ns
ns

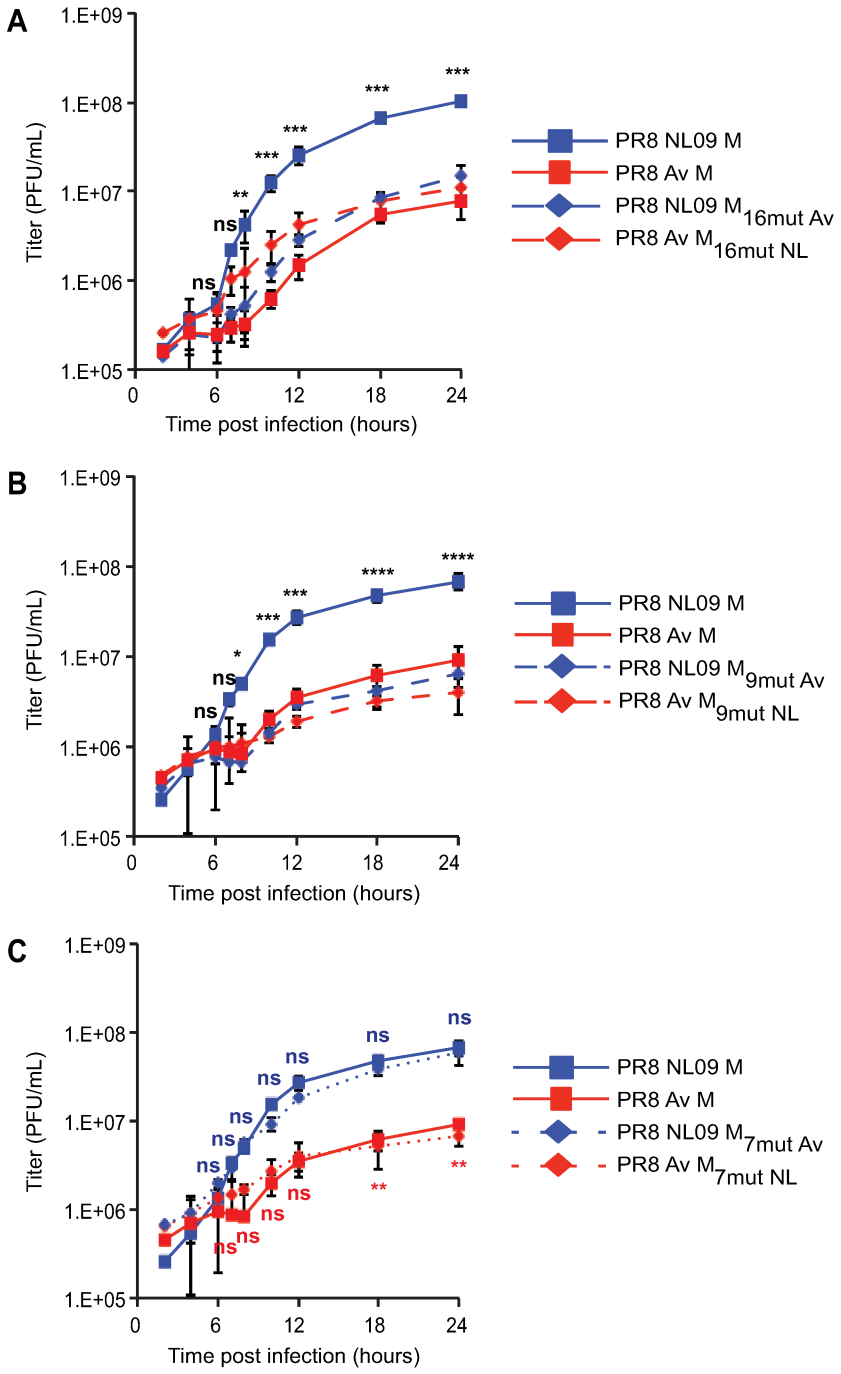
A
1.E+09
1.E+08
1.E+07
1.E+06
1.E+05
Titer (PFU/mL)
0
6
12
18
24
Time post infection (hours)
ns
ns
**
***
***
***
***
PR8 NL09 M
PR8 Av M
PR8 NL09 M16mut Av
PR8 Av M16mut NL
B
1.E+09
1.E+08
1.E+07
1.E+06
1.E+05
Titer (PFU/mL)
0
6
12
18
24
Time post infection (hours)
ns
ns
*
***
***
****
****
PR8 NL09 M
PR8 Av M
PR8 NL09 M9mut Av
PR8 Av M9mut NL
C
1.E+09
1.E+08
1.E+07
1.E+06
1.E+05
Titer (PFU/mL)
0
6
12
18
24
Time post infection (hours)
ns
ns
ns
ns
ns
ns
ns
ns
ns
ns
ns
ns
**
**
PR8 NL09 M
PR8 Av M
PR8 NL09 M7mut Av
PR8 Av M7mut NL

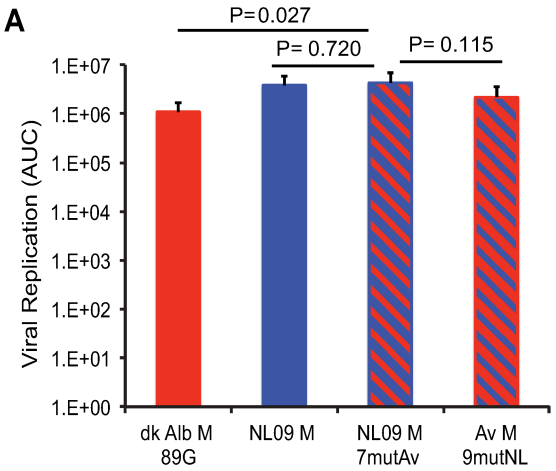
A
P=0.027
P= 0.720
P= 0.115
Viral Replication (AUC)
1.E+07
1.E+06
1.E+05
1.E+04
1.E+03
1.E+02
1.E+01
1.E+00
dk Alb M 89G
NL09 M
NL09 M 7mutAv
Av M 9mutNL

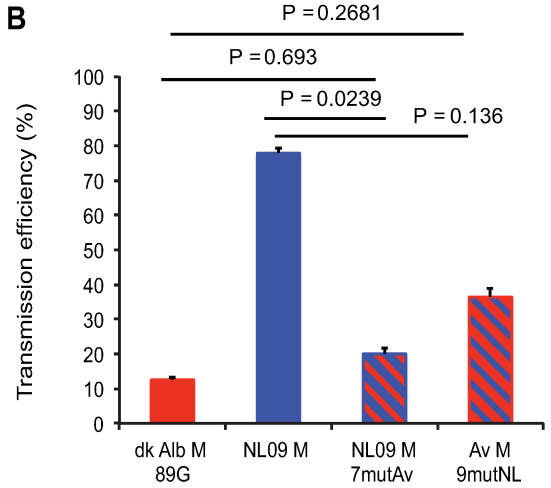
B
P = 0.2681
P = 0.693
P = 0.0239
P = 0.136
Transmission efficiency (%)
100
90
80
70
60
50
40
30
20
10
0
dk Alb M 89G
NL09 M
NL09 M 7mutAv
Av M 9mutNL

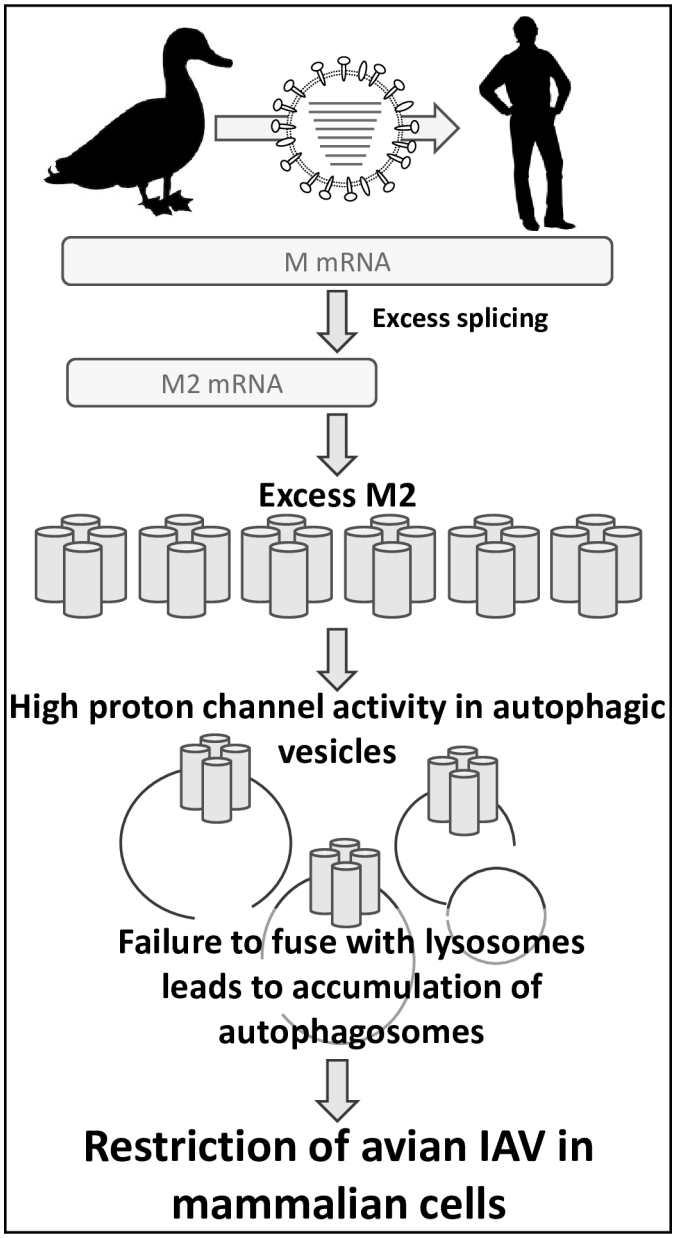
M mRNA
Excess splicing
M2 mRNA
Excess M2
High proton channel activity in autophagic vesicles
Failure to fuse with lysosomes leads to accumulation of autophagosomes
Restriction of avian IAV in mammalian cells